APPLICATIONS OF OZSVÁTH-SZABÓ INVARIANTS TO CONTACT GEOMETRY

David Shea Vela-Vick

A Dissertation

in

Mathematics

Presented to the Faculties of the University of Pennsylvania in Partial Fulfillment of the Requirements for the Degree of Doctor of Philosophy

2009

John B. Etnyre
Supervisor of Dissertation

Tony Pantev
Graduate Group Chairperson

Acknowledgments

First, I would like to thank John Etnyre for being such a great advisor. Thank you for encouraging me to follow my own path, and for supporting me unconditionally, wherever that path led. Thank you, John, for being my mentor and my friend.

I would also like to thank my "second advisor", Herman Gluck, for all that he has done for me the past five years. Herman has shown me that the most productive and enjoyable way to do mathematics is collaboratively with friends and a tin full of cookies.

Thank you to Dennis DeTurck, Connie Leidy, Rafal Komendarczyk, Paul Melvin, Josh Sabloff, Lisa Traynor and Jason Cantarella for years worth of fruitful discussions and encouragement.

I am eternally grateful to Clay Shonkwiler for being my office-mate, editor, computer guru, co-author and overall good friend. Don't think that the calls for help will stop after graduation!

Chris Jankowski, Jen Hom, Dave Fithian, Andrew Obus, Andrew Bressler, Dave Favero, Paul Rowe, Martin Kerin, Pilar Herreros, Mike McDuffee, Wil Brady, Asher Auel, Colin Diemer and John Olsen each played a significant role in making my experience here at Penn so enjoyable.

The PACT crowd out at Bryn Mawr and Haverford has been a wonderful source of support and encouragement the past five years. Special thanks goes to the regulars.

Thank you to the backbone of the Department: Janet Burns, Monica Pallanti, Paula Scarborough and Robin Toney. Without the four of you, surely the department would fall to pieces!

To my parents and grandparents; you inspire me to work hard and live life to its fullest. Thank you for being patient with me and for presenting me with so many opportunities. You may not quite know what I do, but you cheer me on like you do. No words can adequately express how grateful I am to have each of you in my life.

Most of all, thank you to my wonderful and beautiful wife, Monica! More than anyone else, you have been my rock throughout this whole process. Thank you for livening up all the math dinners, and for editing everything I've written...even this. I love you with all my heart!

ABSTRACT

APPLICATIONS OF OZSVÁTH-SZABÓ INVARIANTS TO

CONTACT GEOMETRY

David Shea Vela-Vick

John B. Etnyre, Advisor

Let $T \subset (Y, \xi)$ be a transverse knot which is the binding of some open book, (T, π), for the ambient contact manifold (Y, ξ). We show that the transverse invariant $\widehat{\mathcal{T}}(T) \in \widehat{\mathrm{HFK}}(-Y, K)$, defined in [LOSS08], is nonvanishing for such transverse knots. We also prove a vanishing theorem for the invariants $\mathfrak{L}$ and $\mathfrak{T}$. As a corollary of these two facts, we see that if (T, π) is an open book with connected binding, then the complement of T has no Giroux torsion.

More generally, we prove using different methods that if (B, π) is any open book decomposition of (Y, ξ), then the complement of B is torsion-free.

We also show by explicit computation that the sutured Floer contact invariant can distinguish isotopy classes of tight contact structures on solid tori with convex boundary and $2n$ vertical dividing curves.

Contents

List of Figures

Chapter 1

Introduction

This thesis naturally breaks into two parts. In the first half, we study properties and applications of newly defined invariants of Legendrian and transverse knots. In the second half, we give a direct computation of some contact invariants for contact structures on solid tori with specified boundary conditions. Each of these will be discussed in turn.

1.1 LOSS Invariants and Bindings of Open Books

Lisca, Ozsváth, Stipsicz, and Szabó define a pair of invariants for null-homologous Legendrian and transverse knots in [LOSS08]. These invariants live in the knot Floer homology groups of the ambient space with reversed orientation, and generalize the previously defined invariants of closed contact manifolds, $c(Y,\xi)$. They have been useful in constructing new examples of knot types which are not transversally simple (see [LOSS08, OS08a]).

Here, we compute these invariants for a wide class of transverse knots:

Theorem 1. *Let $T \subset (Y,\xi)$ be a transverse knot which can be realized as the binding of an open book (T,π) compatible with the contact structure ξ. Then the transverse invariant $\widehat{\mathcal{T}}(T)$ is nonvanishing.*

Remark 1.1.1. In [LOSS08], it is shown that if $c(Y,\xi) \neq 0$, then $\mathcal{T}(T) \neq 0$ for any transverse knot $T \subset (Y,\xi)$. In Theorem 1, no restrictions are made on the ambient contact structure ξ. In particular, Theorem 1 is true even when ξ is overtwisted. Moreover, the nonvanishing of the invariant $\widehat{\mathcal{T}}$ implies the nonvanishing of the invariant $\mathcal{T}$.

Let L be a null-homologous Legendrian knot in (Y,ξ). It is shown in [LOSS08] that the invariant $\mathcal{L}(L)$ inside $\mathrm{HFK}^-(-Y,L)$ remains unchanged under negative stabilization, and therefore yields an invariant of transverse knots. If T is a null-homologous transverse knot in (Y,ξ) and L is a Legendrian approximation of T, then $\mathcal{T}(T) := \mathcal{L}(L)$. We will generally state results only in the Legendrian case, even though the same results are also true in the transverse case.

Remark 1.1.2. There is a natural map $\mathrm{HFK}^-(-Y,L) \to \widehat{\mathrm{HFK}}(-Y,L)$, defined by setting $U = 0$. Under this map, the $\mathcal{L}(L)$ is sent to $\widehat{\mathcal{L}}(L)$. Therefore, if $\widehat{\mathcal{L}}(L)$ is nonzero, then $\mathcal{L}(L)$ must also be nonzero. Similarly, if $\mathcal{L}(L)$ vanishes, then $\widehat{\mathcal{L}}(L)$ must also vanish.

In addition to understanding when these invariants are nonzero, we are also interested in circumstances under which they vanish. In [LOSS08], it was shown that if the complement of the Legendrian knot contains an overtwisted disk, then the Legendrian invariant for that knot vanishes. Here, we generalize this result by proving:

Theorem 2. *Let L be a Legendrian knot in a contact manifold (Y,ξ). If the complement $Y - L$ contains a compact submanifold N with convex boundary such that $c(N,\xi|_N) = 0$ in $SFH(-N,\Gamma)$, then the Legendrian invariant $\mathcal{L}(L)$ vanishes.*

Since I-invariant neighborhoods of convex overtwisted disks have a vanishing contact invariant (Example 1 of [HKM07]), Theorem 2 generalizes the vanishing theorem from [LOSS08].

In [GHV07], Ghiggini, Honda, and Van Horn-Morris show that a closed contact manifold with positive Giroux torsion has vanishing contact invariant. They show this by proving that the contact element for a 2π-torsion layer vanishes in sutured Floer homology. Thus, as an immediate corollary to Theorem 2, we have:

Corollary 3. *Let L be a Legendrian knot in a contact manifold (Y, ξ). If the complement $Y - L$ has positive Giroux torsion, then the Legendrian invariant $\mathcal{L}(L)$ vanishes.*

Remark 1.1.3. A similar result has been established for the invariant $\widehat{\mathcal{L}}$ by Stipsicz and Vértesi [SV08] using slightly different arguments.

Remark 1.1.4. Theorem 2 and Corollary 3 are both true in the transverse case as well.

Combining the transverse version of Corollary 3 with Theorem 1, we conclude the following interesting fact about complements of connected bindings:

Theorem 4. *Let (T, π) be an open book with a single binding component. Then the complement of T has no Giroux torsion.*

In joint work with John B. Etnyre [EV08], we extend this result to the case of disconnected bindings, showing:

Theorem 5 (with John B. Etnyre)**.** *Let (B, π) be an open book for a contact manifold (Y, ξ). Then the complement of B has no Giroux torsion.*

Our proof of Theorem 5 is presented in Chapter 5.

1.2 Ozsváth-Szabó Invariants and Contact Structures on Solid Tori

The second part of this thesis is devoted to studying the Heegaard Floer contact invariants for tight contact structures on $S^1 \times D^2$ with convex boundary and $2n$ vertical dividing curves. Tight contact structures on solid tori with convex boundary and $2n$ vertical dividing curves were first classified independently by Giroux in [Gir00] and by Honda in [Hon00]. Our primary goal is to give an alternate proof of this classification using techniques from Heegaard Floer homology. In particular, we show the following:

Theorem 6. *Let ξ_1 and ξ_2 be tight contact structures on a solid torus $S^1 \times D^2$ with convex boundary and $2n$ vertical dividing curves. Then the sutured Floer contact invariants of ξ_1 and ξ_2 agree if and only if they are isotopic as contact structures relative to the boundary.*

Our proof of Theorem 6, found in Chapter 6, is by explicit computation. A list of the potentially distinct tight contact structures on the solid torus with $2n$ vertical dividing curves on the boundary can be obtained using elementary techniques form convex surface theory. To prove Theorem 6, we show that the sutured contact invariants for each of these contact structures are nonzero and pairwise distinct. The hands-on nature of this computation allows for direct comparison of these invariants and yields an explicit proof of Theorem 6.

This same result has been obtained independently by Honda, Kazez and Matić in [HKM08]. There, the authors use contact geometric methods to define a gluing map for sutured Floer homology. By studying properties of this gluing map for certain classes of contact manifolds, the authors indirectly conclude independence of the above mentioned contact invariants.

This thesis is organized as follows: in Chapter 2, we briefly review some of the basic definitions and theorems from contact geometry, Heegaard Floer homology and knot Floer homology. We prove Theorem 1 in Chapter 3 and Theorem 2 in Chapter 4. Next, Chapter 5 is devoted to a proof of Theorem 5 and, finally, we prove Theorem 6 in Chapter 6.

Chapter 2

Background

Here, we discuss the basic definitions and results that are used throughout this thesis. Unless otherwise stated, (Y, ξ) denotes a contact manifold whose contact structure is cooriented. Dividing sets on convex surfaces and sutures on the boundaries of contact manifolds will both be denoted by Γ. In situations where ambiguity may arise, we use subscripts such as Γ_ξ or Γ_Σ for dividing sets to distinguish them from sutures.

2.1 Contact Geometry Preliminaries

Recall that a contact structure on an oriented 3-manifold is a plane field ξ satisfying a certain nonintegrability condition. Since we assume that our plane fields are cooriented, ξ is given as the kernel of some global 1-form: $\xi = \ker(\alpha)$ with $\alpha(N_p) > 0$ for each oriented normal vector N_p to ξ_p. Such an α is called a *contact form for* ξ. In this case, the nonintegrability condition is equivalent to the statement $\alpha \wedge d\alpha > 0$.

A surface $\Sigma \subset (Y, \xi)$ is called *convex* if there exists a contact vector field V for (Y, ξ) such that V is transverse to Σ. The *dividing set* Γ of a convex surface Σ is

$$\Gamma_\Sigma = \{p \in \Sigma \mid V_p \subset \xi\}.$$

Convex surfaces and dividing sets are important because, nearby a convex surface Σ, the contact structure ξ is determined up to isotopy by the dividing set Γ_Σ.

A primary tool used in the study of contact manifolds is Giroux's correspondence between contact structures on 3-manifolds and open book decompositions up to an equivalence called positive stabilization. Indeed, open books lie at the heart of many recent results in contact geometry, and are essential in defining any of the Heegaard Floer contact invariants.

An *open book decomposition* of a contact 3-manifold (Y, ξ) is a pair (B, π), where B is an oriented, fibered, transverse link and $\pi : (Y - B) \to S^1$ is a fibration of the complement of B by oriented surfaces whose oriented boundary is B. The transverse link B is called the *binding* of the open book (B, π), while each of the fiber surfaces $S_\theta = \pi^{-1}(\theta)$ are called *pages*.

An open book is said to be *compatible* with a contact structure ξ if, after an isotopy of the contact structure, there exists a contact form α for ξ such that:

1. $\alpha(v) > 0$ for each (nonzero) oriented tangent vector v to B, and

2. $d\alpha$ restricts to a positive area form on each page of the open book.

Given an open book decompositon of a 3-manifold Y, Thurston and Winkelnkemper [TW75] show how one can produce a compatible contact structure on Y. Giroux proves in [Gir02] that two contact structures which are compatible with the same open book are, in fact, isotopic as contact structures. Giroux also proves that two contact structure are isotopic if and only if they are compatible with open books which are related by a sequence of positive stabilizations.

Alternatively, one can abstractly specify an open book by identifying a surface with boundary S (the page), and a monodromy map $\phi : S \to S$ whose restriction to a neighborhood of ∂S is the identity. Comparing with the first definition of an open book given above, S is the fiber surface $\pi^{-1}(\theta)$, and ϕ as the monodromy map of the fibration π.

A relative version of open book decompositions, called *partial open book decompositions* can be defined for contact manifolds with nonempty, convex boundary. A partial open book decom-

position can be specified by naming a page S, and a partially defined monodromy map $\phi : P \to S$ of a subsurface $P \subset S$. A relative version of Giroux's correspondence theorem holds in this case allowing one to study contact structures on boarded manifolds using open books.

Definition 2.1.1. A knot L smoothly embedded in a contact manifold (Y, ξ) is called *Legendrian* if $T_pL \subset \xi_p$ for all p in L.

Definition 2.1.2. An oriented knot T smoothly embedded in a contact manifold (Y, ξ) is called *transverse* if it always intersects the contact planes transversally with each intersection positive.

We say that two Legendrian knots are *Legendrian isotopic* if they are isotopic through Legendrian knots; similarly, two transverse knots are *transversally isotopic* if they are isotopic through transverse knots. Given a Legendrian knot L, one can produce a canonical transverse knot nearby to L, called the *transverse pushoff* of L. On the other hand, given a transverse knot T, there are many nearby Legendrian knots, called *Legendrian approximations* of T. Although there are infinitely many distinct Legendrian approximations of a given transverse knot, they are all related to one another by sequences of negative stabilizations. These two constructions are inverses to one another, up to the ambiguity involved in choosing a Legendrian approximation of a given transverse knot (see [EFM01, EH01]).

If I is an invariant of Legendrian knots which remains unchanged under negative stabilization, then I is also an invariant of transverse knots: if T is a transverse knot and L is a Legendrian approximation of T, define $I(T)$ to be equal to the invariant $I(L)$ of the Legendrian knot L. This is how the authors define the transverse invariants $\mathcal{T}(T)$ and $\widehat{\mathcal{T}}(T)$ in [LOSS08].

For more on open book decompositions and partial open book decompositions, we refer the reader to [Etn06, Col07] and [HKM07].

2.2 Sutured Floer Homology and the Contact Invariant

In [Juh06], Juhász defined a variant of Heegaard Floer homology for balanced sutured 3-manifolds. This Floer homology theory was used in [HKM07] to define a generalization of the Heegaard-Floer contact invariant for closed contact 3-manifolds (see [OS05a] and [HKM06]).

Suppose that (Y, ξ) is a contact manifold with convex boundary and dividing set Γ_ξ. By thinking of the dividing curves on ∂Y as sutures, (Y, Γ) is naturally a balanced sutured 3-manifold (balanced because ξ is cooriented). The invariant $c(Y, \xi)$, defined by Honda, Kazez and Matić, directly generalizes the original contact invariant defined by Ozsváth and Szabó in [OS05a] and lives in the sutured Floer homology group $\mathrm{SFH}(-Y, -\Gamma)$.

To construct this invariant, let (S, P, ϕ) be a partial open book decomposition of a contact manifold with convex boundary (Y, ξ). Then $Y = S \times [-1, 1]/\sim$, where the equivalence relation $\sim$ is given by

$$(x, t) \sim (x, t') \quad \text{if} \quad x \in \partial S \text{ and}$$

$$(x, 1) \sim (\phi(x), -1) \quad \text{if} \quad x \in P.$$

A *basis* for (S, P) is a collection of properly embedded arcs $\{a_1, \ldots, a_k\}$, contained within the subsurface P, such that after cutting along the a_i, the resulting surface deformation retracts onto $\overline{S - P}$.

Choose such a basis $\{a_1, \ldots, a_k\}$ for (S, P) and construct a second collection of embedded arcs $\{b_1, \ldots, b_k\}$ by applying small isotopies to the a_i's such that their boundaries are isotoped according the orientation on ∂P, and so that each a_i intersects b_i transversally in a single point.

With this data, a sutured Heegaard diagram (Σ, β, α) can be obtained for the $(-Y, -\Gamma_\xi)$.

Namely,

$$\begin{aligned}\Sigma &= (P \times \{1\}) \cup (-S \times \{-1\}) \\ \beta_i &= (b_i \times \{1\}) \cup (\phi(b_i) \times \{-1\}) \\ \alpha_j &= \partial(a_j \times [-1,1]).\end{aligned}$$

Let x_i be the unique intersection point between α_i and β_i on $P \times \{1\}$, and $\mathbf{x} = (x_1, \ldots, x_k)$. It follows immediately from this definition that $\partial\mathbf{x} = 0$. The homology class of $\mathbf{x}$ inside of $\mathrm{SFH}(-Y, -\Gamma)$ is the contact invariant defined in [HKM07]. In what follows, we denote this invariant by $c(Y, \xi)$.

If $L \subset (Y, \xi)$ is a Legendrian link, let $\nu(L)$ denote an open standard neighborhood of L contained in (Y, ξ).

Definition 2.2.1. Denote by $\mathrm{SFH}(L)$ the sutured Floer homology of the balanced sutured 3-manifold $(-(Y - \nu(L)), -\Gamma|_\xi)$. Denote by $c(L)$ the contact invariant of the contact invariant of the contact manifold $(Y - \nu(L), \xi|_{Y-\nu(L)})$.

The invariant $c(L)$ is the Legendrian invariant defined in [HKM07]. Although this invariant is unchanged under Legendrian isotopies of L, it is sensitive to stabilizations (positive and negative) made to the components of L. Indeed, stabilizing a component of the link L may actually change the isomorphism type of the sutured Floer homology theory associated to the Legendrian link. For this reason, $c(L)$ does not also define an invariant of transverse knots or links.

For more on sutured Floer homology and on the sutured contact invariant, see [Juh06, Juh08] and [HKM07, HKM08].

2.3 Invariants of Legendrian and Transverse Knots

Let L be a Legendrian knot with knot type K, and let T be a transverse knot in the same knot type. In [LOSS08], the authors define invariants $\mathcal{L}(L)$ and $\mathcal{T}(T)$ in $\mathrm{HFK}^-(-Y, K)$ and $\widehat{\mathcal{L}}(L)$ and $\widehat{\mathcal{T}}(T)$

in $\widehat{\mathrm{HFK}}(-Y,K)$. These invariants are constructed in a similar fashion to the contact invariants in [HKM06, HKM07]. Below we describe how to construct this invariant for a Legendrian knot.

Let $L \subset (Y,\xi)$ be a null-homologous Legendrian knot. Consider an open book decomposition of (Y,ξ) containing L on a page S. Choose a basis $\{a_0,\dots,a_n\}$ for S (i.e., a collection of disjoint, properly embedded arcs $\{a_0,\dots,a_n\}$ such that $S-\bigcup a_i$ is homeomorphic to a disk) with the property that L intersects only the basis element a_0, and does so transversally in a single point. Let $\{b_0,\dots,b_n\}$ be a collection of properly embedded arcs obtained from the a_i by applying a small isotopy so that the endpoints of the arcs are isotoped according to the induced orientation on ∂S and so that each b_i intersects a_i transversally in the single point x_i. If $\phi : S \to S$ is the monodromy map representing the chosen open book decomposition, then our Heegaard diagram is given by

$$(\Sigma,\alpha,\beta) = (S_{1/2} \cup -S_1, (a_i \cup a_i), (b_i \cup \phi(b_i))).$$

The first basepoint, z, is placed on the page $S_{1/2}$ in the complement of the thin strips of isotopy between the a_i and b_i. The second basepoint, w, is placed on the page $S_{1/2}$ inside the thin strip of isotopy between a_0 and b_0. The two possible placements of w correspond to the two possible orientations of L.

The Lengendrian invariant $\mathcal{L}(L)$ is defined, up to isomorphism, to be the element $[\mathbf{x}] = [(x_0,\dots,x_n)]$ in $\mathrm{HFK}^-(\Sigma,\beta,\alpha,w,z)$. A picture of this construction is given in Figure 3.4. If T is a transverse knot, the transverse invariant $\mathcal{T}(T)$ is defined to be the Legendrian invariant of a Legendrian approximation of T.

Interestingly, these invariants do not necessarily vanish for knots in overtwisted contact manifolds; this is why we do not need to assume tightness in Theorem 1. Another property, which will be useful in Chapter 3, is that these invariants are natural with respect to contact $(+1)$-surgeries.

Theorem 2.3.1 (Ozsváth-Stipsicz, [OS08a]). *Let $L \subset (Y,\xi)$ be a Legendrian knot. If (Y_B,ξ_B,L_B) is obtained from (Y,ξ,L) by contact $(+1)$-surgery along a Legendrian knot B in (Y,ξ,L), then,*

under the natural map

$$F_B : \mathrm{HFK}^-(-Y, L) \to \mathrm{HFK}^-(-Y_B, L_B),$$

$\mathcal{L}(L)$ *is mapped to* $\mathcal{L}(L_B)$.

An immediate corollary of Theorem 2.3.1 is the following:

Corollary 2.3.2. *Let $L \subset (Y, \xi)$ be a Legendrian knot, and suppose that (Y_B, ξ_B, L_B) is obtained from (Y, ξ, L) by Legendrian surgery along a Legendrian knot B in (Y, ξ, L). If $\mathcal{L}(L) \neq 0$ in $\mathrm{HFK}^-(-Y, L)$, then $\mathcal{L}(L_B) \neq 0$ in $\mathrm{HFK}^-(-Y_B, L_B)$.*

Remark 2.3.3. Theorem 2.3.1 and Corollary 2.3.2 are also true for the invariant $\widehat{\mathcal{L}}(L)$ and for the invariants $\mathcal{T}(T)$ and $\widehat{\mathcal{T}}(T)$ in the case of a transverse knot.

In addition, the invariant $\mathcal{L}$ directly generalizes the original contact invariant $c(Y, \xi) \in \widehat{\mathrm{HF}}(-Y)$ (see [OS05a]). Under the natural map $\mathrm{HFK}^-(-Y, L) \to \widehat{\mathrm{HF}}(-Y)$ obtained by setting $U = 1$, $\mathcal{L}(L)$ maps to $c(Y, \xi)$, the contact invariant of the ambient contact manifold.

We encourage the interested reader to look at [LOSS08, OS08a] to learn about other properties of these invariants.

2.4 The c-Bar Invariant

A connection between the HKM Legendrian invariant and the LOSS Legendrian/transverse invariant was explored by Stipsicz and Vertesi in [SV08]. As a first step towards developing this connection, Stipsicz and Vertesi show that $c(L)$ can be mapped to an intermediate invariant which we presently call the c-bar invariant, denoted by $\overline{c}(L)$. It is this bar invariant that Stipsicz and Vertesi are able to directly identify with the Legendrian/transverse invariant from [LOSS08].

We will see in Chapter 5 that this intermediate bar invariant is very useful in its own right. It is defined for any Legendrian knot or link and does not require any of the preconditions, like being null-homologous, that are required to define the invariants $\mathcal{L}(L)$ and $\widehat{\mathcal{L}}(L)$.

Consider a Legendrian knot $L \subset (Y, \xi)$, and let $\nu(L) \subset (Y, \xi)$ be an open standard neighborhood of L. Focusing our attention on the complement of this standard neighborhood, we consider the contact manifold obtained by attaching a basic slice to the torus boundary of $(Y - \nu(L), \xi|_{Y-\nu(L)})$ so that the resulting dividing set on the new boundary consists of precisely two meridional (measured with respect to the original knot L) dividing curves.

We denote this new contact manifold by $\overline{Y}(L)$. A local picture of this construction is supplied in Figure 2.1(a). The contact invariant of the manifold $\overline{Y}(L)$ is an invariant of the Legendrian knot L. We denote this invariant by $\overline{c}(L)$, and the sutured Floer homology of the ambient manifold by $\overline{\mathrm{SFH}}(L)$.

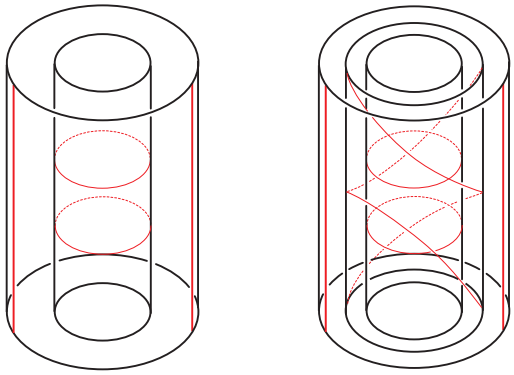

(a) (b)

Figure 2.1: Obtaining $\overline{Y}(L)$ and factor tori

As was observed in [SV08], $\overline{c}(L)$ is invariant under negative stabilizations of L. Recall that if L and L' differ by a negative stabilization, then the complements of open standard neighborhoods of L and L' differ by a basic slice attachment. As depicted in Figure 2.1(b), the basic slice attachment that yields $\overline{Y}(L)$ factors into two basic slice attachments. The first attachment corresponds to the stabilization $L \rightsquigarrow L'$, and the second corresponds to the attachment yielding $\overline{Y}(L') = \overline{Y}(L)$.

Chapter 3

The LOSS Invariants and Bindings of Open Books

Let $T \subset (Y, \xi)$ be a transverse knot. Recall that Theorem 1 states that if T is the binding for some open book (T, π) for (Y, ξ), then the transverse invariant $\widehat{\mathcal{T}}(T) \in \widehat{\mathrm{HFK}}(-Y, T)$ is nonvanishing.

In this Chapter, we prove Theorem 1 in three steps. In Section 3.1 we construct an open book on which a Legendrian approximation L of the transverse knot T sits. Then we show in Section 3.2 that the Heegaard diagram obtained in Section 3.1 is weakly admissible. Finally, in Section 3.3, we prove the theorem in the special case where the monodromy map ϕ_n consists of a product of n negative Dehn twists along a boundary-parallel curve.

An arbitrary monodromy map differs from some such ϕ_n by a sequence of positive Dehn twists, or Legendrian surgeries, along curves contained in pages of the open book. By Corollary 2.3.2, since the transverse invariant is nonvanishing for the monodromy maps ϕ_n, it must also be nonvanishing for an arbitrary monodromy map.

3.1 Obtaining the Pointed Diagram

By hypothesis, T is the binding of an open book (T, π) for (Y, ξ). In order to compute the transverse invariant $\widehat{\mathcal{T}}(T)$, we need to find a Legendrian approximation L of T, realized as a curve on a page of an open book for (Y, ξ).

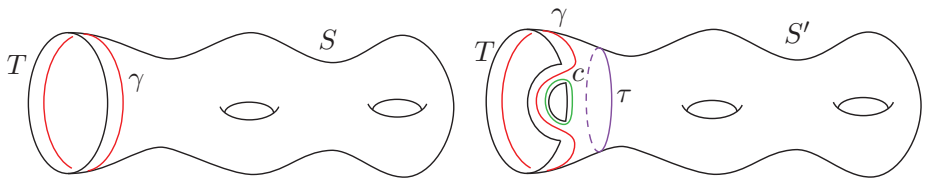

(a) (b)

Figure 3.1: The open book (T, π) and its stabilization

In Figure 3.1(a), we see a page of the open book (T, π). Here, T appears as the binding $\partial S = T$. Assuming the curve γ could be realized as a Legendrian curve, it would be the natural choice for the Legendrian approximation L. Unfortunately, since γ is zero in the homology of the page, γ cannot be made Legendrian on the page.

To fix this problem, stabilize the diagram. The result of such a stabilization is illustrated in Figure 3.1(b). To see that this solves the problem, we prove the following lemma:

Lemma 3.1.1. *The stabilization depicted in Figure 3.1(b) can be performed while fixing T as the "outer" boundary component.*

Assume the truth of Lemma 3.1.1 for the moment. Then the curve γ depicted in Figure 3.1(b) can now be Legendrian realized, as it now represents a nonzero element in the homology of the page. By construction, if we orient this Legendrian coherently with T, then T is the transverse pushoff of γ.

Proof. Consider S^3 with its standard tight contact structure. Let (H_+, π_+) be the open book for (S^3, ξ_{std}) whose binding consists of two perpendicular Hopf circles and whose pages consist

of negative Hopf bands connecting these two curves. In this case, each binding component is a transverse unknot with self linking number equal to -1.

Let T be a transverse knot contained in a contact manifold (Y, ξ) and let U be a transverse unknot in $(S^3, \xi|_{\text{std}})$ with self-linking number equal to -1. Observe that the complement of a standard neighborhood of a point contained in U is itself a standard neighborhood of a point contained in a transverse knot. Therefore, if we perform a transverse connected sum of T with the transverse unknot of self linking number equal to -1 in (S^3, ξ_{std}), we do not change the transverse knot type of T.

(a) (b)

Figure 3.2: Murasugi summing along a bigon

Let (B, π) be an open book with connected binding for a contact manifold (Y, ξ). Consider the contact manifold obtained from (Y, ξ) by Murasugi summing the open book (B, π) with the open book (H_+, π_+) along bigon regions bounded by boundary-parallel arcs contained in pages of the respective open books. The summing process is depicted in Figure 3.2. Figure 3.2(a) shows the open books before the Murasugi sum, while Figure 3.2(b) shows the resulting open book after the sum.

The Murasugi sum operation has the effect of performing a contact connected sum of (Y, ξ) with (S^3, ξ_{std}) and a transverse connected sum of the binding component B with one of the binding components of H_+ (see [Tor00]). Before and after pictures of this operation are shown in Figures 3.3(a) and 3.3(b), respectively. Since both of the binding components of the open book (H_+, π_+) are transverse unknots with self linking number equal to -1, this connected sum has no effect on the transverse knot type of the "outer" boundary component of the open book in Figure 3.1. $\square$

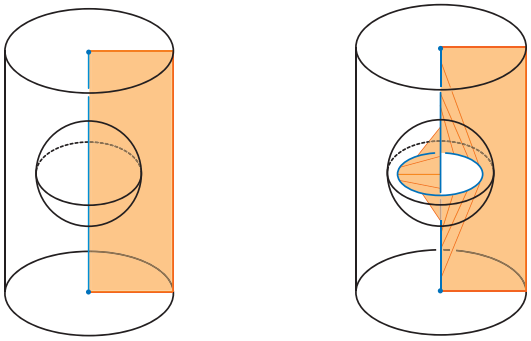

(a) (b)

Figure 3.3: A Murasugi sum with (H_+, π_+) along a bigon region

Since the curve γ can now be Legendrian realized and approximates T as desired, we will denote γ by L from this point forward. The new monodromy map $\phi' : S' \to S'$ is equal to the old monodromy map, ϕ, composed with one positive Dehn twist along the curve c shown in Figure 3.1(b). For notational ease, we continue denoting the monodromy map by ϕ, and the page by S.

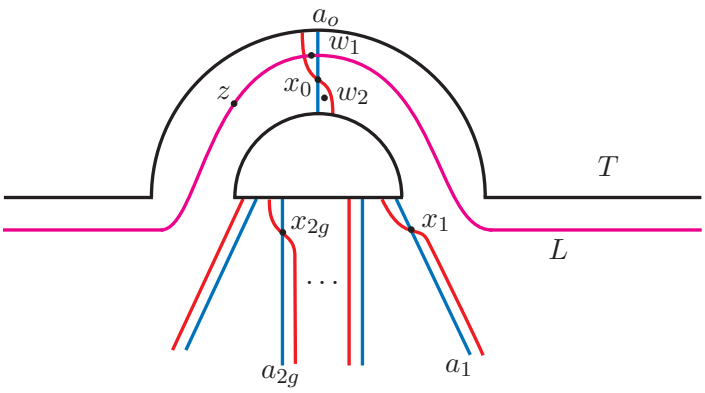

Figure 3.4: An appropriate choice of basis

We choose a basis for our surface whose local picture near the stabilization is depicted in Figure 3.4. There are two possible choices for the placement of the second basepoint w: w_1 and w_2. In order for L to be oriented coherently with T, we must choose $w = w_1$.

3.2 Admissibility

In this section, we construct a weakly admissible, doubly-pointed Heegaard diagram from the open book described in Section 3.1.

Before we continue, let us discuss some notation. We are concerned with open book decompositions whose pages are twice-punctured surfaces. We picture a genus g surfaces as a $4g$-sided polygon with certain boundary edges identified. We choose the standard identification scheme, where the first and third edges are identified, as are the second and fourth edges, the fifth and seventh edges, and so on. For convenience, we always assume that the first edge appears in the 12 o'clock position, at the top of each diagram.

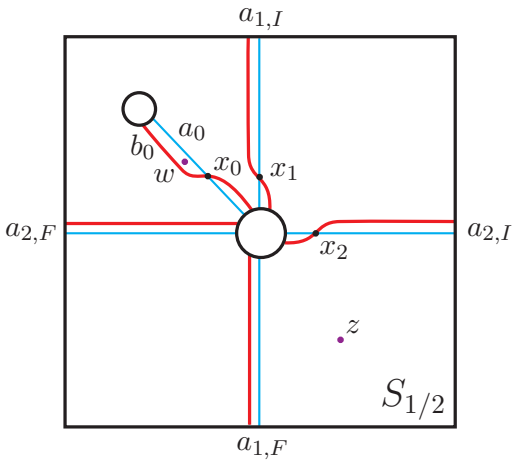

Figure 3.5: The page $S_{1/2}$

Our punctures are always situated so that one of the punctures is in the center of the polygon, with the other close by. We choose our basis elements, $a_1, \ldots, a_{2g}$, to be straight arcs emanating from the center of the polygon and passing out the corresponding edge. If we were to forget about the identifications being made at the boundary, the basis element a_i would break into two straight arcs emanating from the center of the diagram. For ease of exposition in what follows, we label the first segment that we see as we move clockwise around the diagram $a_{i,I}$, and the second $a_{i,F}$. The subscript I stands for "initial", while the subscript F stands for "final".

According to these conventions, the second boundary component of our surface lies in the region between the curves $a_{2g,F}$ and $a_{1,I}$. The last basis element a_0 is a straight line segment connecting the two boundary components of the surface.

We have adopted the practice of Honda, Kazez and Matić of placing surrogate basepoints throughout the diagram whenever it is convenient. The points signal that no holomorphic disk is allowed to cover that region of the diagram.

We have restricted our figures to the case where our page is a twice-punctured torus, and our monodromy map ϕ consists of two negative Dehn twists along the curve τ in Figure 3.1(b). The resulting doubly-pointed Heegaard diagram is shown in Figures 3.5 and 3.6.

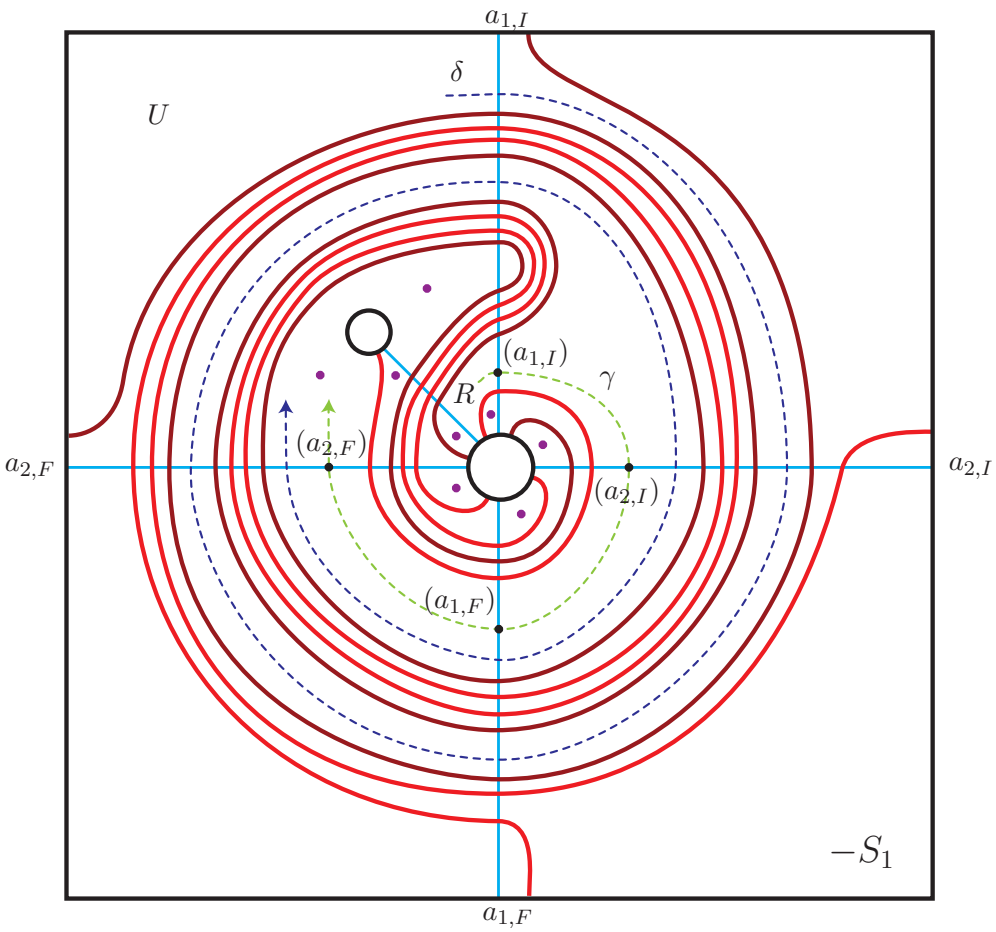

Figure 3.6: The page $-S_0$

Figure 3.5 shows the $S_{1/2}$ page of our open book, while Figure 3.6 shows the $-S_1$ page (note the reversed orientation). The invariant appears in Figure 3.5 as the intersection point $\mathbf{x} = (x_0, x_1, x_2)$.

Consider the small region southeast of x_0 in Figure 3.5. This region is equal to the region R in Figure 3.6. Let γ be the dashed arc connecting the region R to the z-pointed region. Denote by $(a_{i,*})$, the intersection point between $a_{i,*}$ and γ.

Lemma 3.2.1. *The doubly-pointed Heegaard diagram described above, and appearing in Figures 3.5 and 3.6, is weakly admissible.*

Proof. Let P be a periodic domain for the pointed Heegaard diagram $(\Sigma, \beta, \alpha, w)$. Suppose P has nonzero multiplicity in the z-pointed region. Without loss of generality, we assume that this multiplicity is $+1$. In particular, the multiplicity of the region just above the point $(a_{2,F})$ in Figure 3.6 is $+1$. In order for the w-pointed region to have multiplicity zero, the α_0- and β_0-curves must be contained in the boundary of the periodic domain P and must appear with multiplicity ± 1 (depending on the chosen orientations of α_0 and β_0). This forces the small region southeast of x_0 in Figure 3.5 to have multiplicity $+2$. Since this region is the same as the region R in Figure 3.6, R must also have multiplicity $+2$.

Consider the dashed arc γ connecting R to the z-pointed region. In order for P to exist, the multiplicities of the regions intersected by γ must go from $+2$ in the region R to $+1$ in the z-pointed region.

However, the curve γ intersects each α-curve (other than α_0) in two points, each with opposite sign. The boundary of a periodic domain must be a sum of full α- and β-curves, so if the multiplicity increases (or decreases) by a factor of n as γ passes one of the intersection points, it must decrease (or increase) by that same factor as γ passes the other intersection point. Therefore, the net change in multiplicity of the periodic domain P along γ between the region R and the z-pointed region is zero. We have seen that the multiplicity of the region R is $+2$, whereas the multiplicity of the z-pointed region was assumed to be $+1$. From this contradiction, we conclude

that P must have multiplicity zero in the z-pointed region.

Since each α- and each β-curve bound the z-pointed region on either side, and since P has multiplicity zero in the z-pointed region, we conclude that P must have positive and negative coefficients. □

3.3 Computing $\widehat{\mathfrak{T}}(T)$

Let $\mathbf{x} = (x_0, \ldots, x_{2g})$; we show that the transverse invariant $\widehat{\mathfrak{T}}(T) = [(x_0, \ldots, x_{2g})]$ is nonzero. To prove this, we show that the set $\pi_2(\mathbf{y}, \mathbf{x})$ has no holomorphic representatives unless $\mathbf{y} = \mathbf{x}$, in which case we have only the trivial holomorphic disk. This is equivalent to showing that, if we reverse the roles of the α- and β-curves, $\pi_2(\mathbf{x}, \mathbf{y})$ has no holomorphic representatives for all $\mathbf{y} \neq \mathbf{x}$.

Let $\mathbb{D}$ be a holomorphic representative of some homotopy class $\phi \in \pi_2(\mathbf{y}, \mathbf{y}')$ with $n_z(\phi) = 0$. As is common in Heegaard Floer homology, we consider the "shadow" of $\mathbb{D}$ on our Heegaard surface Σ. This shadow is a sum of regions in the complement of the α- and β-curves, and is denoted $D = \sum_i c_i D_i$. Because everything in this story is holomorphic, each of the c_i are nonnegative.

Suppose R_1 and R_1 are two adjacent regions in a Heegaard diagram (i.e., R_1 and R_2 share an edge), and D is as above. In general, the multiplicities of R_1 and R_2 can differ arbitrarily. In our case, however, the multiplicities of any two adjacent regions can differ by at most one. This is true because each of the α- and β-curves in a Heegaard diagram coming from an open book decomposition bound the z-pointed region to either side. Therefore, the boundary of any such region D can never contain a full α or β curve, and the multiplicities of R_1 and R_2 can differ by at most one.

Consider the region R in Figure 3.6, and the curve γ connecting R to the z-pointed region.

Lemma 3.3.1. *The net change in multiplicity between the region R and the z-pointed region along γ is nonnegative.*

Proof. The proof of Lemma 3.3.1 is similar to the proof of the admissibility lemma in Section 3.2.

Recall that the curve γ intersects each α_i-curve in two points: $(a_{i,I})$ and $(a_{i,F})$. We show that if the multiplicity of the regions intersected by γ decrease by a factor of -1 at the point $(a_{i,I})$, then there must be a corresponding increase in multiplicity at the point $(a_{i,F})$. Similarly, we show that if the multiplicity of the regions intersected by γ decrease by a factor of -1 at the point $(a_{i,F})$, then there must be a corresponding increase in multiplicity at the point $(a_{i,I})$.

Observe that the multiplicity along γ cannot decrease as γ passes over the point $(a_{1,I})$. Recall that we are only considering holomorphic disks which emanate from the intersection point $(x_0, \ldots, x_{2g})$. Thus, if there is a decrease in multiplicity at $(a_{1,I})$, a segment of the α_1-curve between the intersection point $(a_{1,I})$ and x_1 must be contained in the boundary of the holomorphic disk. Looking at the diagram in Figure 3.6, we see that any such arc has z-pointed region to the west, contradicting its existence.

In the genus one case, a similar argument shows that there can be no decrease in multiplicity at the point $(a_{2,I})$. So assume that either the genus of S is greater than one, or that we are considering an intersection point (a) beyond $(a_{2,I})$ along γ.

Suppose that $(a) = (a_{i,I})$, and that the multiplicity along γ decreases by a factor -1 as it passes over at the point (a). Then the segment of the α_i-curve beginning at the point (a) and traveling away from the center of the diagram to the point x_i is contained in the boundary of the holomorphic disk. This implies that the region just past the intersection point $(a_{i,F})$ along γ gains a $+1$ boost in multiplicity. Therefore, the increase in multiplicity at the point $(a_{i,F})$ balances the decrease in multiplicity at the point $(a_{i,I})$.

Similarly, if $(a) = (a_{i,F})$ and if the multiplicity along γ decreases by a factor of -1 as γ passes over (a), then the segment of the α_i-curve beginning at the point $(a_{i,I})$ and traveling away from the center of the diagram to the point x_i is contained in the boundary of the holomorphic disk. This implies that the region just past the intersection point $(a_{i,I})$ gains a $+1$ boost in multiplicity. Thus, the decrease in multiplicity at the point $(a_{i,F})$ is balanced by the increase in multiplicity at the point $(a_{i,I})$.

Since each decrease in multiplicity along γ is balanced by a corresponding increase in multiplicity somewhere else along γ, we have that the net change in multiplicity between the region R and the z-pointed region along the curve γ is nonnegative. □

Consider the region U in Figure 3.6, and the curve δ connecting U to the z-pointed region. By an argument similar to the proof of Lemma 3.3.1, we have the following:

Lemma 3.3.2. *The net change in multiplicity between the region U and the z-pointed region along δ is nonnegative.*

□

Proof of Theorem 1. There are two main cases to consider.

Case 1: Assume that the holomorphic disk emanating from $\mathbf{x} = (x_0, \ldots, x_{2g})$ is nonconstant near the intersection point x_0. In this case, the region R in Figure 3.6 has multiplicity $+1$. By Lemma 3.3.1, this implies that the multiplicity of the z-pointed region must be at least $+1$, a contradiction.

Case 2: Now suppose that the holomorphic disk is constant at the point x_0, meaning that the multiplicity of the region R is zero. We investigate the possible ways that holomorphic disks can emanate from the center of Figure 3.6.

Suppose, for the moment, that all the regions bordered by the β_0-curve have zero multiplicity. Then a holomorphic disk emanating from the center of Figure 3.6 is (locally) constrained to lie within the strip bounded by the darkened portions of the β-curves.

In order for this to be the case, the boundary of the disk must have veered off the α-curves while still contained within this strip. Therefore, all the α-curves are "used up" close to the center of the diagram (i.e., by the time they first intersect a darkened β-curve). This, in turn, forces the multiplicity of the region U in Figure 3.6 to be positive.

By Lemma 3.3.2, this implies that the multiplicity of the z-pointed region must be positive, a contradiction. Therefore, in order for such a nontrivial holomorphic disk to exist, at least one of

the regions bordered by β_0 must have nonzero multiplicity.

Recall that in Case 2 we are assuming that the holomorphic disk is constant near x_0. This means that the curve β_0 cannot be involved in the boundary of the holomorphic disk, so at least one of the regions intersected by γ must have positive multiplicity. Let R' be the first region along γ with positive multiplicity, and let (a) be the $(a_{i,*})$ immediately preceding R'.

If $(a) = (a_{i,F})$, then by an argument similar to the proof of Lemma 3.3.1, it can be shown that the net change in multiplicity between the region R' and the z-pointed region must be nonnegative. The fact that (a) is a final point ensures that there can be no decrease in multiplicity at the point $(a_{i,I})$ since, by the definition of R', the regions to both sides of this point have multiplicity zero.

On the other hand, suppose $(a) = (a_{i,I})$. An argument similar to that in Lemma 3.3.1 demonstrates that for each decrease in multiplicity, there is a corresponding increase in multiplicity, except possibly at the point $(a_{i,F})$. If the multiplicity decreases at the point $(a_{i,F})$, then the segment of the α_i-curve from $(a_{i,F})$ to (a) must be contained in the boundary of the holomorphic disk. This then implies that the multiplicity of the region U is at least one.

Again, by Lemma 3.3.2, this forces the multiplicity of the z-pointed region to be positive, a contradiction. □

This completes the proof of Theorem 1.

Chapter 4

A Vanishing Theorem for the LOSS Invariants

In this chapter, we prove Theorem 2. The proof in this case is very similar to the proof of Theorem 4.5 in [HKM07]. The key differences are that we must include the Legendrian knot L when choosing a Legendrian skeleton for the complement of the submanifold N, and that we must be cautious about the changes made to the diagram in the spinning process used to make the diagram strongly admissible.

Proof of Theorem 2. We begin by constructing a partial open book decomposition for the contact submanifold $(N, \xi|_N)$, which can be extended to an open book decomposition for all of (Y, ξ). Following [HKM07], we must show that the basis $\{a_1, \ldots, a_r\}$ for the partial open book decomposition of $(N, \xi|_N)$ can be extended to a basis $\{a_1, \ldots, a_r, a'_0, a'_1, \ldots, a'_s\}$ for the extended open book decomposition of (Y, ξ), where $L \cap (\bigcup a_i \cup \bigcup a'_j) = L \cap a'_0 = 1\text{pt}$.

Claim: We may assume without loss of generality that the complement of N is connected.

Proof of claim. Let (M, ξ) be a compact manifold with possibly nonempty boundary, and let $(M', \xi|_{M'})$ be a compact submanifold of (M, ξ) with convex boundary. In [HKM08], the authors show that the vanishing of the contact invariant for $(M', \xi|_{M'})$ implies the vanishing of the contact invariant for (M, ξ).

Suppose the complement of N is disconnected. Then, since $c(N, \xi|_N) = 0$, the contact manifold obtained by gluing the components of $Y - N$ not containing L to N must also have vanishing contact invariant. In particular, we may assume without loss of generality that $Y - N$ is connected.

□

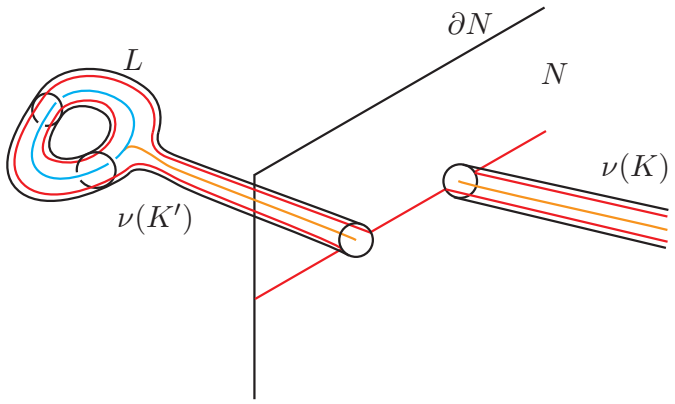

Figure 4.1: Choosing a Legendrian skeleton

Let K be a Legendrian skeleton for N, and let K' be an extension of the Legendrian knot L to a Legendrian skeleton for $N' = Y - N$ (see Figure 4.1). Assume that the univalent vertices of K and K' in ∂N do not intersect.

The Legendrian skeleton K gives us a partial open book decomposition for $(N, \xi|_N)$. Let $\nu(K)$ be a standard neighborhood of K inside of N, and let $\nu(K')$ be a standard neighborhood of K' inside of $Y - N$. We can build an open book decomposition for all of Y by considering the the handlebodies $(N' - \nu(K')) \cup \nu(K)$ and $\nu(K') \cup (N - \nu(K))$. By construction, each of these handlebodies are disk decomposable. A page S of the open book for (Y, ξ) is constructed from the page of the partial open book for $(N, \xi|_N)$ by repeatedly attaching 1-handles away from the

portions of the open book coming from the boundary of $\nu(K)$. A picture of this construction is depicted in Figure 4.2.

In Figure 4.2, the portion of the page S coming from the boundary of N is shown in black, and has its boundary lines thickened. The portion of S coming from the boundary of $\nu(K)$ is lightly colored (orange), and appears in the lower right portion of the figure. Finally, the portion of S coming from the extension of the open book to all of Y is also lightly colored (green), and appears in the lower left corner of the figure.

Let $\{a_1, \ldots, a_n\}$ be a basis for the partial open book coming from $(N, \xi|_N)$, and let ϕ be the corresponding partially defined monodromy map for this open book. Consider a new partial open book, whose page is equal to S, and whose partially defined monodromy map is equal to ϕ. Because this new partial open book only differs from the partial open book coming from $(N, \xi|_N)$ by handle attachments away from $\partial\nu(K)$, the contact element for this new partial open book vanishes along with $c(N, \xi|_N)$.

Since $Y - N$ is connected, the basis $\{a_1, \ldots, a_n\}$ can, after a suitable number of stabilizations, be extended to a basis for all of Y.

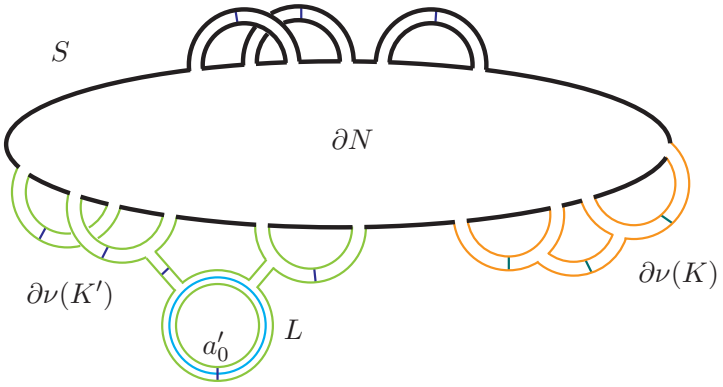

Figure 4.2: Viewing the resulting open book decomposition

By construction, the new monodromy map ϕ' extends ϕ, the monodromy map for N. We can see our Legendrian knot L on the page S. The local picture around $L \subset S$ (shown in blue) must

look like that in Figure 4.2.

As was observed in [LOSS08], the "spinning" isotopies needed to make this Heegaard diagram strongly admissible can be performed on the portion of the Heegaard diagram coming from the page S_1. This changes the monodromy map ϕ', but only within its isotopy class.

If we delete the α- and β-curves coming from $\{a'_0, a'_1, \ldots, a'_s\}$, then we are left with a diagram which is essentially equivalent to that coming from the partial open book (S, ϕ), but whose monodromy has been changed by an isotopy. Since altering the monodromy map by an isotopy cannot change whether or not the contact element vanishes in sutured Floer homology, we know that the contact element corresponding to the partial open book (S, ϕ') vanishes. That is, if $\mathbf{x} = (x_1, \ldots, x_n)$, then there exist c_i and $\mathbf{y}_i$ such that $\partial(\sum_i c_i \mathbf{y}_i) = \mathbf{x}$ in the sutured Floer homology of the manifold obtained from the partial open book (S, ϕ').

Let $\mathbf{x}' = (x'_0, x'_1, \ldots, x'_s)$; we claim that $\partial(\sum_i c_i(\mathbf{y}_i, \mathbf{x}')) = (\mathbf{x}, \mathbf{x}')$ in $\mathrm{HFK}^-(-Y, L)$. The intersection points coming from $\mathbf{x}'$ must map to themselves via the constant map. This allows us to ignore the α- and β-curves corresponding to these intersection points, leaving us with a diagram which is essentially equivalent to the partial open book (S, ϕ'). $\square$

Chapter 5

$\mathcal{C}$-Bar and Bindings of Open Books

In this chapter, we prove Theorem 5. The effort in this proof is in showing that if (B, S) is an open book decomposition of a given contact manifold (Y, ξ), then the invariant $\overline{c}(B)$ is nonvanishing. Having established this, it follows easily from Ghiggini, Honda and Van Horn-Morris's vanishing theorem [GHV07] that the complement of B must be torsion-free.

Proof of Theorem 5. Let (B, S) be an open book decomposition for the contact manifold (Y, ξ), and let L_B be any Legendrian approximation of B. We must show that the contact manifold $(\overline{Y}(L_B), \overline{\xi}_{L_B})$, constructed in Section 2.4, has nonvanishing contact invariant.

As an intermediate step in proving $c(\overline{Y}(L_B), \overline{\xi}_{L_B})$ is nonzero, we prove the following lemma:

Lemma 5.0.3. *The contact manifold $(\overline{Y}(L_B), \overline{\xi}_{L_B})$ is tight.*

Proof of Lemma 5.0.3. To show that $(\overline{Y}(L_B), \overline{\xi}_{L_B})$ is tight, we apply the Colin gluing theorem (see [Col99]).

Colin's gluing theorem states that if (Y_1, ξ_1) and (Y_2, ξ_2) are two universally tight contact manifolds, and $T_i \subset Y_i$ are pre-Lagrangian, incompressible tori, then the contact manifold obtained by gluing Y_1 to Y_2 along T_1 and T_2 is universally tight.

Suppose for the moment that the binding B has a single component, and let T be the convex torus bounding $(Y - \nu(L_B), \xi|_{Y-\nu(L_B)})$. The contact manifold $(\overline{Y}(L_B), \overline{\xi}_{L_B})$ is obtained from $(Y - \nu(L_B), \xi|_{Y-\nu(L_B)})$ by attaching a basic slices to the boundary torus T.

As observed in Section 2.4, this basic slice attachment factors as a composition of two basic slice attachments. The first such attachment corresponds to a negative stabilization of L_B

$$(Y - \nu(L_B), \xi|_{Y-\nu(L_B)}) \rightsquigarrow (Y - \nu(L'_B), \xi|_{Y-\nu(L'_B)}),$$

while the second corresponds to the attachment,

$$(Y - \nu(L'_B), \xi|_{Y-\nu(L'_B)}) \rightsquigarrow (\overline{Y}(L'_B), \overline{\xi}_{L'_B}) = (\overline{Y}(L_B), \overline{\xi}_{L_B}).$$

Inside this first basic slice, we can find a pre-Lagrangian torus T' parallel to the original boundary component T. The complement of this pre-Lagrangian torus has two components; the first diffeomorphic to $T^2 \times I$, and the other to $\overline{Y - B}$.

The contact structure restricted to either of these subspaces is universally tight. In the case of $T^2 \times I$, this is true because it sits as a subspace of a basic slice, a universally tight contact manifold. In a similar spirit, the second component is contained in complement of the binding, $(Y - B, \xi|_{Y-B})$, which is also universally tight.

In general, the binding B consists of many components. In that case, we apply the above argument inductively to each of the basic slice attachments yielding the contact manifold $(\overline{Y}(L_B), \overline{\xi}_{L_B})$, concluding that the result is universally tight.

All that remains to be checked before we can inductively apply the Colin gluing theorem is that each of the boundary tori $T_i \subset \partial\,\overline{(Y - B)}$ are incompressible.

To see that each T_i is incompressible, we consider its preimage inside the universal cover of $Y - \nu(B)$. We claim that each preimage is homeomorphic to a copy of $\mathbb{R}^2$, immediately implying incompressibility.

Recall that $Y - \nu(B)$ is a surface bundle over S^1, fibered by oriented surfaces S_θ, whose oriented boundary is B. Consider first the intermediate cover which unwraps the S^1-factor. This cover is

homeomorphic to $S \times \mathbb{R}$. In this intermediate cover, the preimage of each T_i is a cylinder.

The universal cover of $Y - \nu(B)$ is homeomorphic to the universal cover of S crossed with the real line $\mathbb{R}$. Passing to the full universal cover, we see that the preimage of each of the above cylinders is homeomorphic to $\mathbb{R}^2$.

This shows that each of the T_i are incompressible, finishing the proof of Lemma 5.0.3. □

Knowing that the contact manifold $(\overline{Y}(L_B), \overline{\xi}_{L_B})$ is tight, we can proceed with showing that its contact invariant is nonvanishing.

As we saw in Chapter 3, the Legendrian approximation L_B can be chosen so that the twisting of the contact planes with respect to the framing induced on each component of L_B by the fiber surface S is -1. In this case, the local picture around each boundary component of $(\overline{Y}(L_B), \overline{\xi}_{L_B})$ is shown in Figure 5.1(a).

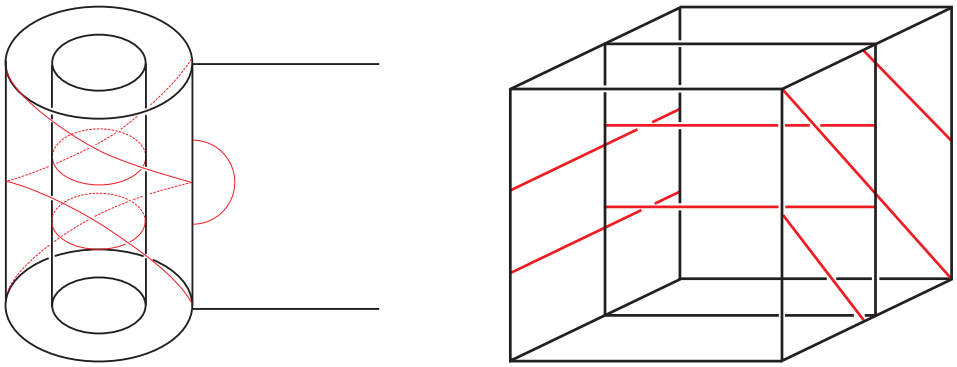

(a) (b)

Figure 5.1: Constructing $\overline{Y}(L_B)$ and viewing factor tori

In this case, observe that the dividing set on a convex annulus extending the page S to the meridian-sloped boundary component consists, up to isotopy, of two horizontal dividing curves (see Figure 5.1(b)). Denote by S' the extension of the convex surface S by this convex annulus.

The dividing set on S^1 consists of a collection of boundary-parallel dividing curves; one for each boundary component of $\overline{Y}(L_B)$. Such a surface is called *well-groomed*.

It was shown in [HKM07] that if (Y_2, ξ_2) is obtained from (Y_1, ξ_1) by cutting along a well-groomed convex surface, then the contact invariant of (Y_2, ξ_2) is nonvanishing if and only if the contact invariant of (Y_1, ξ_1) is nonvanishing. Therefore, to prove Theorem 1, it suffices to show that the contact manifold obtained by cutting along S' is nonzero.

Cutting along S', we obtain the tight contact manifold (Y', ξ'), whose dividing set is shown in Figure 5.2.

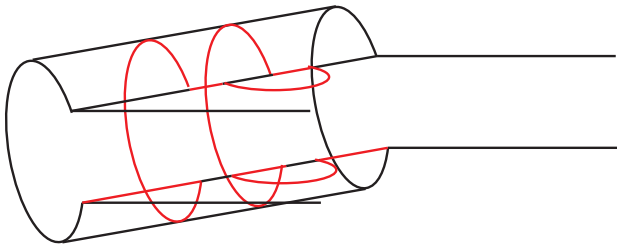

Figure 5.2: Splitting $\overline{Y}(L_B)$ along a page

This contact manifold with convex boundary is diffeomorphic to the surface $S' \times [0, 1]$. The dividing set is isotopic to the collection of curves $\partial S' \times 1/2$.

Tight contact structures on such manifolds are unique. These contact structures are deformations of foliations, and embed into closed, Stein fillable contact manifolds. Since the contact invariant for closed manifolds is nonvanishing for Stein fillable manifold, it must be the case that the sutured contact invariant for the contact manifold (Y', ξ') is nonvanishing.

This finishes the proof and shows that $\overline{c}(B) \neq 0$.

□

Chapter 6

Sutured Floer Homology and Contact Structures on Solid Tori

Consider two tight contact structures ξ_1 and ξ_2 on a solid torus with convex boundary and $2n$ vertical dividing curves. Theorem 6 states that ξ_1 and ξ_2 are isotopic as contact structures if and only if $c(\xi_1) = c(\xi_2)$ inside the sutured Floer homology group $\mathrm{SFH}(-(S^1 \times D^2), -\Gamma_{2n})$.

We can understand such contact structures by focusing on convex meridional disks $D \subset (S^1 \times D^2, \xi_{2n})$. Since the contact structures we are interested in are tight, the dividing set on any such D cannot contain embedded simple closed curves. Therefore it consists of precisely n properly embedded arcs connecting $2n$ distinguished points on the boundary of D (points on ∂D which intersect the dividing set Γ_{2n}). Call such a collection of properly embedded arcs on a disk an *admissible dividing set*.

The following proposition establishes a relationship between contact structures on solid tori with the above boundary conditions and dividing sets on convex meridional disks.

Proposition 6.0.1. *Let ξ_1 and ξ_2 be contact structures on $S^1 \times D^2$ with convex boundary and $2n$ vertical dividing curves, and suppose that D_1 and D_2 are convex meridional disks for ξ_1 and ξ_2*

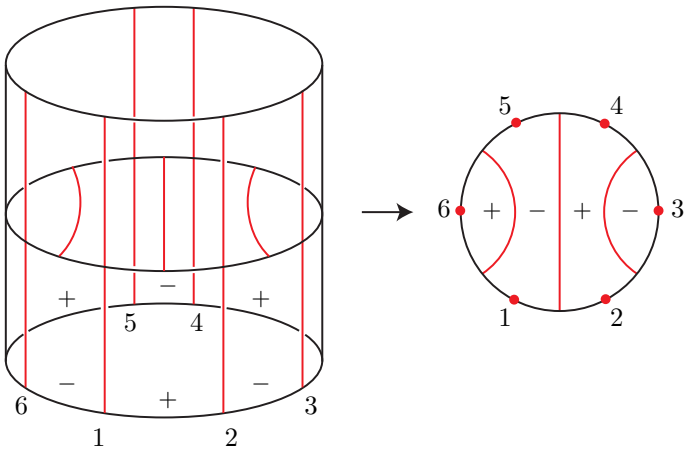

Figure 6.1: Convex meridional disks

respectively. If dividing sets on D_1 and D_2 are isotopic and if each ξ_i is tight in the complement of D_i, then ξ_1 and ξ_2 are isotopic.

Proof. Observe that there exists an isotopy ϕ_t of $S^1 \times D^2$ which fixes each of the dividing curves on $T = \partial(S^1 \times D^2)$ as a set and, at time one, maps D_1 to D_2. We can further assume that ϕ_1 is a contactomorphism of standard open neighborhoods $N(D_i \cup T)$. That is,

$$\phi_1 : N(D_1 \cup T) \to N(D_2 \cup T)$$

is a diffeomorphism, and

$$\phi_{1*}\xi_1|_{N(D_1 \cup T)} = \xi_2|_{N(D_2 \cup T)}.$$

Since $\xi_1' = \phi_{1*}\xi_1$ and ξ_2 agree on $N(D_2 \cup T_2)$, after cutting along D_2 and rounding corners, we get two tight contact structures ξ_1' and ξ_2 on the ball B^3 with convex boundary. All such tight contact structures are isotopic, implying that the contact structures ξ_1' and ξ_2 are isotopic away from $D_2 \cup T$, finishing the proof.

□

Remark 6.0.2. For each admissible dividing set Γ, there exists a contact structure ξ on $S^1 \times D^2$ such that,

- Γ as the dividing set on a convex meridional disk $D \subset (S^1 \times D^2, \xi)$, and
- after cutting along D and rounding corners, the result is a tight contact structure with convex boundary on the ball B^3.

Proposition 6.0.1 asserts that this induced contact structure is unique up to a contact isotopy preserving the dividing curves on $\partial(S^1 \times D^2)$.

Figure 6.2 depicts the collection of all possible admissible dividing sets in the case $n = 3$.

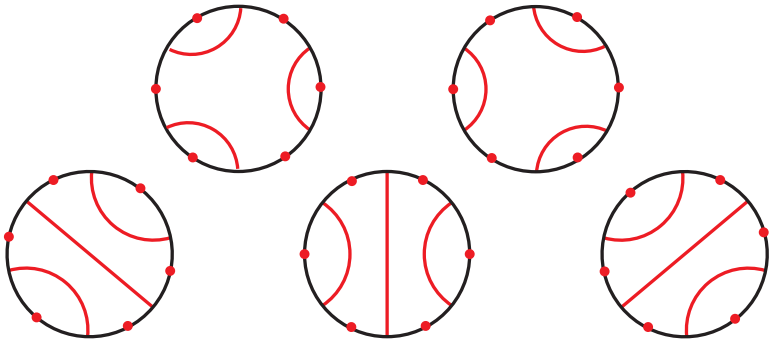

Figure 6.2: Possible dividing sets on convex meridional disks when $n = 3$

Giroux and Honda independently proved the converse to Proposition 6.0.1, establishing a one-to-one correspondence between the set tight contact structures on solid tori with $2n$ vertical dividing curves and the set of admissible dividing sets on convex meridional disks. For example, combining their result with the enumeration given in Figure 6.2, we see that there are precisely 5 distinct tight contact structures on $(S^1 \times D^2, \Gamma_6)$ up to isotopy.

We aim to proof of this fact directly using Heegaard Floer homology. This is accomplished by explicitly computing the contact invariants for each of the (potentially) tight contact structures on $(S^1 \times D^2, \Gamma_{2n})$. After confirming that each contact invariant is nonvanishing (verifying tightness of all relevant contact structures), we show that they are all pairwise distinct.

6.1 Obtaining a Partial Open Book

The first step in our proof is to generate partial open book decompositions and, in turn, sutured Heegaard diagrams for $(-(S^1 \times D^2), -\Gamma_{2n})$ corresponding to each admissible dividing set on a convex meridional disk D. This construction is identical to that in [HKM07].

Fix a dividing set Γ on D, and let ξ_{2n} be the contact structure on $S^1 \times D^2$ induced by Γ. A Legendrian skeleton for $(S^1 \times D^2, \xi_{2n})$ is obtained by choosing a suitable graph $\mathfrak{G}_D$ contained in D.

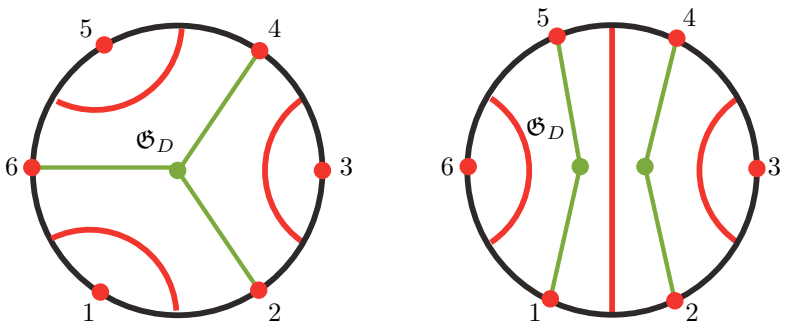

Figure 6.3: Obtaining the graph $\mathfrak{G}_D$

Each component of $\overline{D - \Gamma}$ is naturally a $2m$-gon. For each $2m$-gon which is not a bigon, there is, unique up to isotopy, a tree which has a single interior vertex, one "boundary vertex" on each of the m-boundary edges not contained in Γ, and m-edges beginning at the interior vertex and terminating at each of the boundary vertices. Denote the union of such trees in D by $\mathfrak{G}_D$ (See Figure 6.3).

Since each component of $D - \mathfrak{G}_D$ contains elements of the dividing set Γ, we can apply the Legendrian realization principle to make $\mathfrak{G}_D$ Legendrian (see [Etn06]). Removing a standard open tubular neighborhood of $\mathfrak{G}_D$ from $(S^1 \times D^2, \xi_{2n})$, the the subdisks of D give a disk decomposition of the result. Figure 6.4 depicts such disk decompositions in two main $n = 3$ cases.

From this disk decomposition, we can apply the method described in [HKM07] to obtain a partial open book (S, P, ϕ) for $(S^1 \times D^2, \xi_{2n})$. The partial open books resulting from the disk

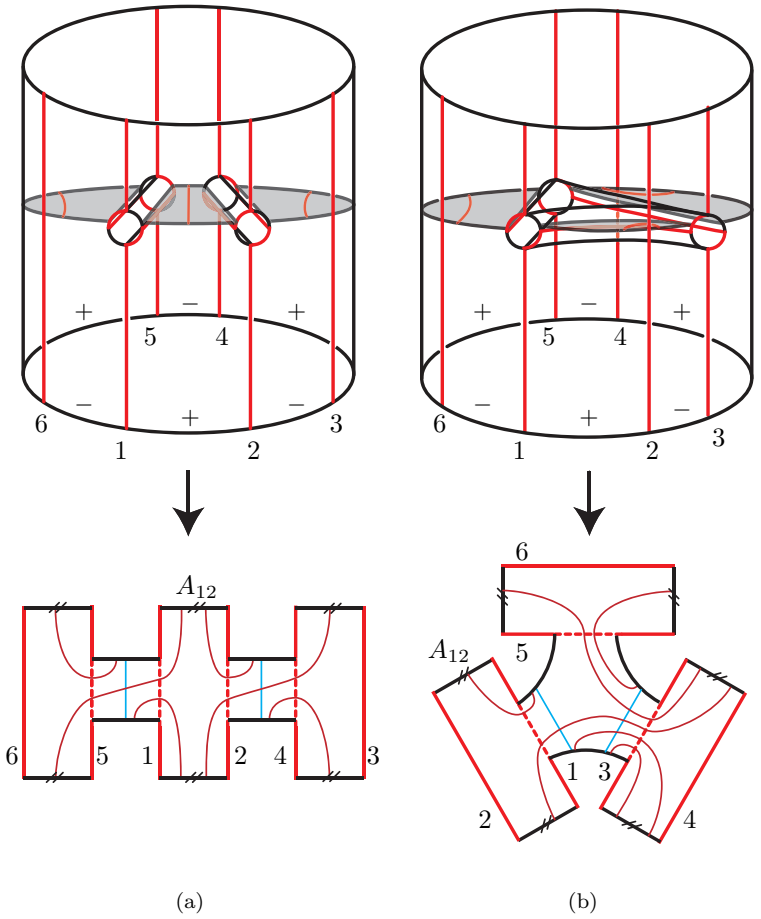

Figure 6.4: Choosing a Legendrian skeleton and the resulting partial open book

decompositions in Figure 6.4 are shown in the lower portion of that same figure.

Given an admissible dividing set Γ on D, denote the partial open book decomposition obtained by applying the above procedure to the pair (D, Γ) by (S_D, P_D, ϕ_D). The subsurface P_D consists of a disjoint union of polygons, one for each component of the graph $\mathfrak{G}_D$. The page S_D is a union of annuli connected to one another by components the subsurface P_D. Each annulus intersects at least one, but no more than two component of P_D.

The next step is to choose a basis for the subsurface P_D. Beginning with the simplest case first, let (S, P, ϕ) be the partial open book obtained by applying the above algorithm to a convex meridional disk with dividing set consisting of k boundary parallel curves. In this case, P has a single component and the page S is equal to P with k annular strips glued to every other boundary edge.

The basis $\{a_1, \ldots, a_{k-1}\}$ consists of properly embedded arcs in P parallel to the annular components of S. One arc is placed next to the annular strip A_{12}, which is boarded by the number 1 and 2 sutures. From there, arcs are placed in counterclockwise order around P.

As discussed in Chapter 2, the contact invariant is specified by the (unique) collection of intersection points $(x_1, \ldots, x_k)$ between the β and α curves on the "top copy" (hidden from view) of the subsurface P.

In this restricted case, where the dividing set Γ_D consists solely of boundary-parallel arcs, we call the resulting sutured Heegaard diagram a *basic initial diagram*. Note that a basic initial diagram comes equipped with an identification of the A_{12} annular component or, equivalently, an identification of the number 1 and 2 boundary sutures.

Abstractly, partial open books yielding basic initial diagrams can be iteratively glued together along their annular components, creating a "tree" of sorts. If P_i is a component of P, define the *distance* from P_i to A_{12} to be the minimum number of components of P intersected by an arc beginning inside P_i and terminating in A_{12}.

After identifying the annular component A_{12}, the basis choice convention can then be extended

to this more general setting. First, we choose a basis on the distance-one components of P (i.e., the components of P whose boundaries intersect A_{12}). As before, basis arcs will consist of properly embedded arcs parallel to the annular components of S. Place arcs parallel to A_{12} and extend counterclockwise as before. Next, we consider the distance-two components of P. By the constructing of (S, P), each such component is connected by a unique annular strip to a distance one component of P. Place an arc parallel to this annular component, and extend counterclockwise as before. Now repeat this procedure for all the distance-three components, and so on.

The resulting sutured Heegaard diagram, together with an identification of the number 1 and 2 sutures is called an *initial diagram*.

An alternate example in the case $n = 7$ is shown in Figure 6.5. In this example, we start with a dividing set on a convex meridional disk and immediately report the resulting initial diagram.

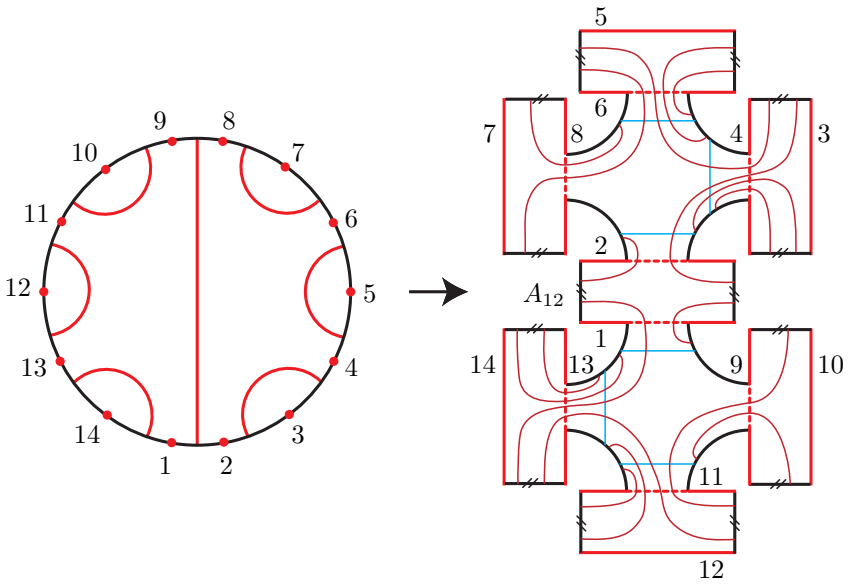

Figure 6.5: Obtaining a partial open book from a convex meridional disk

We see immediately that the Heegaard diagrams generated from convex meridional disks according to the above described procedure are examples of initial diagrams.

Observation 1: All initial diagrams come from a unique admissible dividing set on a convex meridional disk. In other words, there is a one-to-one correspondence between the set of admissible

dividing sets on convex meridional disks and the set of abstract initial diagrams.

The identification of the number 1 and 2 sutures determines a numbering on all the remaining sutures in an initial diagram. Vice versa, identifying the intersections of the number 1 and 2 boundary sutures with a convex meridional disk D removes any rotational ambiguity in the dividing set on D.

This first observation allows us to refocus our attention on particular diagrams, and show that their corresponding contact invariants are pairwise distinct.

6.2 Standard Diagrams Part One

We now begin describing a handle-slide algorithm whose input is an initial diagram (see Section 6.1), and whose output is a fixed sutured Heegaard diagram for $(-S^1 \times D^2, -\Gamma_{2n})$.

To distinguish each of the relevant contact invariants, they must be simultaneously realized on a common sutured Heegaard diagram. This common diagram is depicted in Figure 6.6. The effort in subsequent sections is devoted to tracking the contact element through the various maps induced by the handle-slides transforming a given initial diagram into standard form.

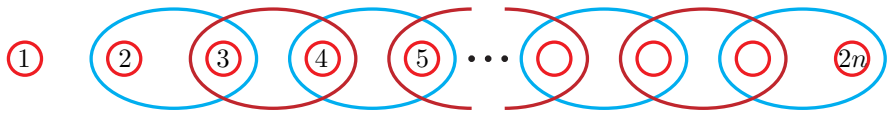

Figure 6.6: A sutured Heegaard diagram in standard form

Focusing once again on a simple case first, consider an initial diagram which is built by gluing together two basic initial diagrams along the A_{12} annular component, like the one shown in the upper left portion of Figure 6.7.

Any initial diagram specifies a sutured Heegaard diagram, whose Heegaard surface Σ is topologically a $2n$-punctured sphere with one boundary component for each suture. Choose a point p in the center of A_{12}, then stereographically project Σ from p to the plane $\mathbb{R}^2$. An example of

the resulting Heegaard diagram in the case at hand is shown in the upper right corner of Figure 6.7. After an isotopy, we obtain the somewhat simpler diagram shown in the lower portion of Figure 6.7.

We have identified the collection of intersection points between the lightly colored (blue) α curves and the dark colored (maroon) β curves corresponding to the contact invariant by black dots, a convention we will continue whenever possible.

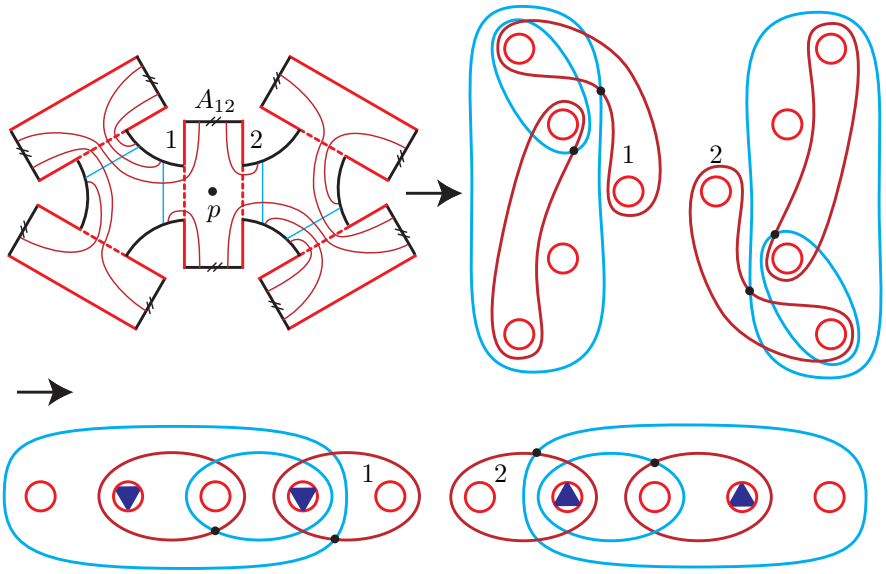

Figure 6.7: Construction of a basic H1-diagram

This sutured Heegaard diagram, together with this collection of intersection points is called a *stage one H1-diagram*. The portion of a stage one initial diagram to the right of the number one suture is a *basic H1-diagram*. The *length* of a basic H1-diagram is the number of α (or β) it contains.

Note that after identifying the 1 and 2 boundary sutures (dividing curves), by the placement of the α and β curves and the ordering of the dividing curves along the boundary of $S^1 \times D^2$, the numbering on the remaining sutures in a stage one H1-diagram is uniquely determined.

In Figure 6.7, some of the regions bounded by sutures have been decorated with solid (purple)

triangles. We call these regions *receiving regions*. Their purpose will shortly become apparent.

In the general case, an initial diagram is built by gluing together many basic initial diagrams and identifying the annular strip A_{12}. In this case, we apply the exact same procedure. First, we choose a point p at the center of the annular strip A_{12}. Next, we stereographically project from p onto the plane $\mathbb{R}^2$ and simplify the result as above.

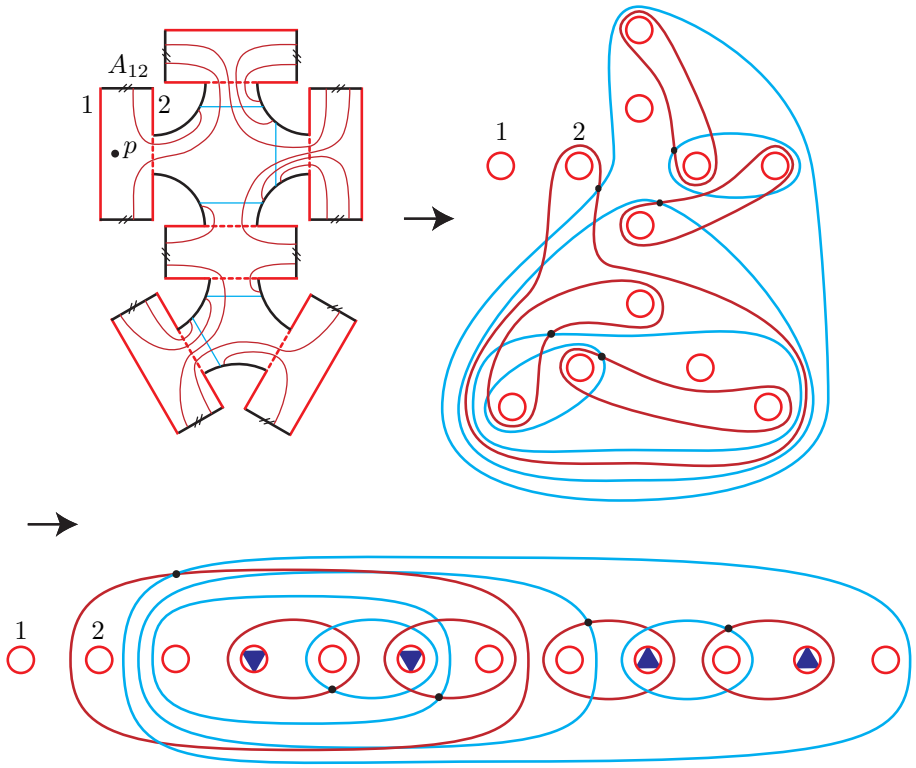

Figure 6.8: Construction of an H1-diagram

Figure 6.8 depicts an example where the initial diagram consists of an $n = 3$ basic initial diagram glued to an $n = 4$ basic initial diagram along the second annular boundary component (according to the counterclockwise ordering used in Section 6.1). Following the above procedure, we see that the result is stage one H1-diagram with the first receiving suture on the right-hand side replaced by the inversion of a length two basic H1-diagram.

An *H1-diagram* is a sutured Heegaard diagram together with a collection of distinguished

intersection points $\mathbf{x}$ which is built from a stage one H1-diagram by iteratively replacing receiving sutures by the inversions of positive length basic H1-diagrams. The following observation is immediate.

Observation 2: There is a one-to-one correspondence between the set of abstract initial diagrams and the set of abstract H1-diagrams.

6.3 Admissibility

In what follows, we consider many different Heegaard double and triple diagrams. For our arguments to hold, admissibility of each diagram is essential. Because the relevant Heegaard surfaces possess many boundary components, the weak admissibility of each diagram is evident.

We leave this as a straightforward exercise to the reader with the following hint: any α- or β-which bounds regions with boundary sutures on both sides cannot itself be contained in the boundary of a periodic domain with all positive or all negative coefficients.

6.4 Nonvanishing of the Contact Invariants

We can now conclude that each of the contact invariants under consideration are nonzero. Because of the abundance of sutures in each H1-diagram, the boundary map for such a Heegaard diagram is identically zero. Therefore, every collection of intersection points, including the contact element, which pairs the α and β curves represents a nonzero element in sutured Floer homology.

This, in particular, implies that any contact structure induced by an admissible dividing set on a convex meridional disk *MUST* be tight.

6.5 Standard Diagrams Part Two

We now begin a simplification process that will transform an H1-diagram to standard form.

The essential content of this section is captured in Figures 6.9 and 6.10. The top portion of Figure 6.9 depicts a basic H1-diagram. The lower portion of this figure is obtained from the top by handle-sliding the outermost (blue) curve α_0 repeatedly over all other α curves until it becomes α_0', swallowing only the two rightmost receiving suture and boundary suture.

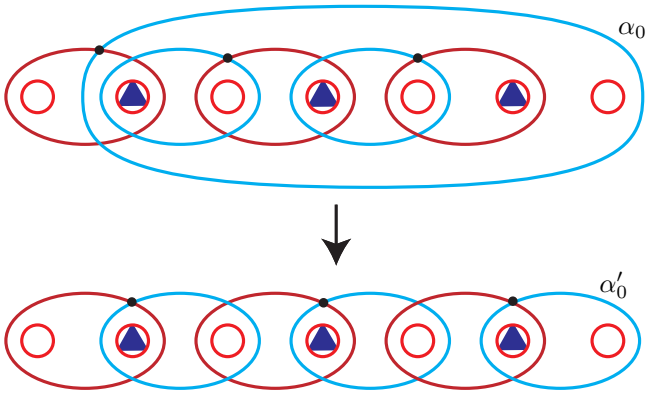

Figure 6.9: Simplifying a basic H1-diagram

For such a sutured Heegaard diagram, consider the distinguished collection of "upper" intersection points. Call the result of this sequence of handle-slides applied to a basic H1-diagram, together with the collection of "upper" intersection points a *basic H2-diagram*.

This process can be generalized to an arbitrary H1-diagram in the following way. Order the basic H1-diagrams constituting a given H1-diagram lexicographically, first by stage, then by their left-to-right order in the diagram. Now, in lexicographic order, apply the above sequence of handle-slides to each basic H1-diagram.

An example of this procedure is illustrated in Figure 6.10.

The resulting sutured Heegaard diagram, together with the obvious distinguished collection of intersection points is called an *H2-diagram*. Abstractly, an H2-diagram can be constructed in stages by iteratively replacing receiving sutures with inversions of basic H2-diagrams.

Observation 3: There is a one-to-one correspondence between the set of $H1$-diagrams and the set of abstract $H2$-diagrams.

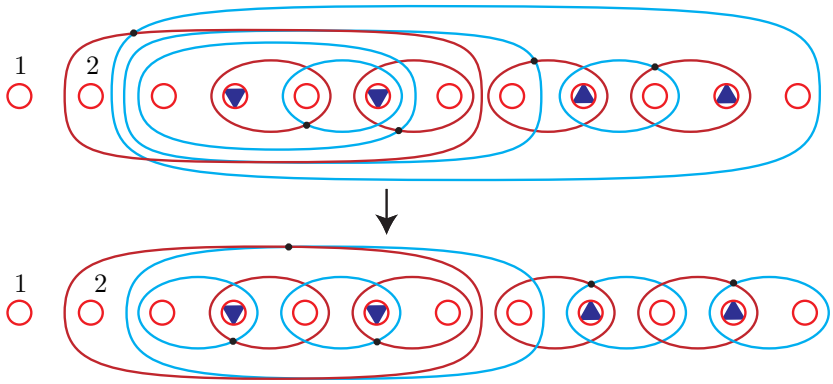

Figure 6.10: Simplifying an H1-diagram

Our task now shifts to understanding how the contact invariant maps under the above sequence handle-slides.

Lemma 6.5.1. *Under the maps induced by the above handle-slides, the contact invariant is identified with the distinguished collection of intersection points in the resulting H2-diagram.*

Proof. Given an H1-diagram $(D, \mathbf{x})$, let $(D_1, \mathbf{x}_1), \dots (D_\ell, \mathbf{x}_\ell)$ be a lexicographic enumeration of the basic H1-diagrams constituting $(D, \mathbf{x})$. Our proof is by induction on this collection of basic H1-diagrams.

Let $j \geq 1$ be given, and suppose that the handle-slide algorithm has been successfully applied to $(D_i, \mathbf{x}_i)$ for $i < j$, and no intersection points have been changed for $i > j$.

Consider the first handle-slide applied to $(D_j, \mathbf{x}_j)$. We can view the corresponding Heegaard triple by looking at its restrictions to $(D_i, \mathbf{x}_i)$ for each i. For $i = j$, a representative picture of this Heegaard triple is given in Figure 6.11(a). If $i > j$, the restriction of the corresponding Heegaard triple to $(D_i, \mathbf{x}_i)$ is depicted in Figure 6.12(a). Similarly, if $i < j$, Figure 6.12(b) depicts the corresponding Heegaard triple restricted to $(D_i, \mathbf{x}_i)$.

These pictures are completely accurate, up to the length of a given $(D_i, \mathbf{x}_i)$. It is straightforward to check that the only holomorphic triangle with corners at θ and at the contact invariant is the one shown. In particular, almost all the triangles are forced to be small triangles, with the

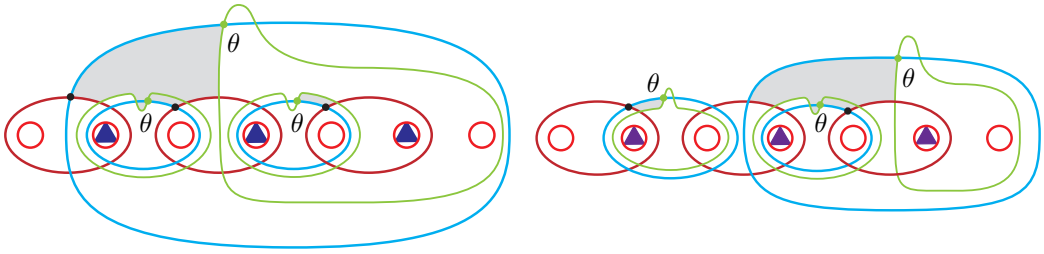

(a) $(D_j, \mathbf{x}_j)$, first handle-slide (b) $(D_j, \mathbf{x}_j)$, second handle-slide

Figure 6.11: Holomorphic triangles for $(D_j, \mathbf{x}_j)$

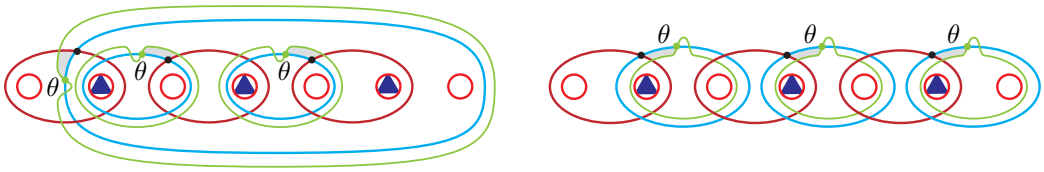

(a) $(D_i, \mathbf{x}_i)$, $i > j$ (b) $(D_i, \mathbf{x}_i)$, $i < j$

Figure 6.12: Other holomorphic triangles for the H1 to H2 handle-slides

Figure 6.11(a) depicting the only exception.

Similar arguments apply as we continue to handle-slide this α curve further. Representative pictures of subsequent Heegaard triple diagrams are obtained by combining Figure 6.11(b) for $(D_j, \mathbf{x}_j)$ and Figures 6.12(a) and 6.12(b) for $(D_i, \mathbf{x}_i)$ where $i \neq j$. Again, these figures are completely accurate up to the length of each $(D_i, \mathbf{x}_i)$.

This completes the proof of Lemma 6.5.1

□

We finish this section by noting that each H2-diagram falls into one of three classes. In the first class, the number 1 suture is isolated in the "unbounded" region of $\mathbb{R}^2$ (as in Figure 6.8). In the second class, we have H2-diagrams where the number 2 suture is isolated in the "unbounded" region of $\mathbb{R}^2$ (as would be the case if we generated an H2-diagram from the basic initial diagram in Figure 6.4(b)). The last class consists of diagrams where neither the number 1 nor 2 sutures are contained in the unbounded region (as in Figure 6.7).

In Sections 6.6 through 6.8, we focus our attention on only the first of these three classes. The information gathered in these sections will then be used to complete the proof of Theorem 6 in Section 6.9.

6.6 Standard Diagrams Part Three

This section discusses the next step in the simplification process. We emphasize that the handle-slides discussed in this section only involve α and β curves in the *first two stages* of the H2-diagram obtained in Section 6.5. In particular, all α and β curves coming from basic H2-diagrams in stages two and lower are fixed under these handle-slides.

Figure 6.13 depicts two diagrams. The first is an example of an H2-diagram from the previous section (sans intersection points). The second is an alternate sutured Heegaard diagram, obtained from the first by a sequence of handle-slides taking β_0 to β_0' and α_0 to α_0'.

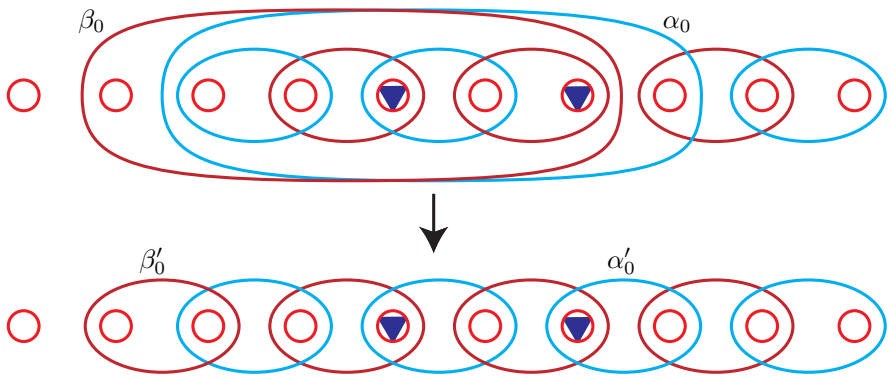

Figure 6.13: Combining stages one and two of an H2-diagram

First, the β_0 curve in the first stage of this H2-diagram is handle-slid "leftward" over each of the β curves contained in its receiving region. This process is then repeated for the α_0 curve, now handle-sliding it "rightward" over all the α curves in that same receiving region. In the end, this process yields the sutured Heegaard diagram shown at the bottom of Figure 6.13.

This process is repeated (when applicable) for each of the other first stage α and β curves

whose enclosed receiving region contains a positive length basic H2-diagram. In the end, the first and second stages of the original H2-diagram are combined into a single first or "top" level portion of the sutured Heegaard diagram. As before, our task shifts to understanding how the contact invariant maps under this sequence of handle-slides.

The computation in this case is similar to that in Lemma 6.5.1. Let $(D, \mathbf{x})$ be a given H2-diagram, and let $\{(D_i, \mathbf{x}_i)\}$ be the basic H2-diagrams constituting $(D, \mathbf{x})$, ordered lexicographically. Then $(D_1, \mathbf{x}_1)$ is the sole stage one basic H2-diagram, $(D_2, \mathbf{x}_2), \ldots, (D_k, \mathbf{x}_k)$ are the stage two basic H2-diagrams, and $(D_{k+1}, \mathbf{x}_{k+1}), \ldots, (D_\ell, \mathbf{x}_\ell)$ are the rest.

The first in this sequence of handle-slides involves sliding a β curve from $(D_1, \mathbf{x}_1)$ over a β curve in $(D_2, \mathbf{x}_2)$. A representative picture of this portion of the resulting Heegaard triple diagram is shown in Figure 6.14(a). For $i > 2$, the Heegaard triple diagram restricted to $(D_i, \mathbf{x}_i)$ is similar to Figure 6.14(c). As in the proof of Lemma 6.5.1, these figures are completely accurate up the the lengths of a given $(D_i, \mathbf{x}_i)$.

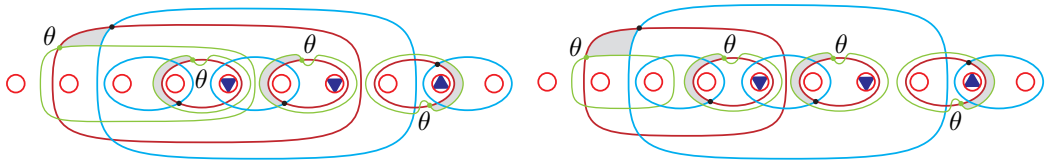

(a) $(D_1, \mathbf{x}_1)$ and $(D_2, \mathbf{x}_2)$, first handle-slide

(b) $(D_1, \mathbf{x}_1)$ and $(D_2, \mathbf{x}_2)$, second handle-slide

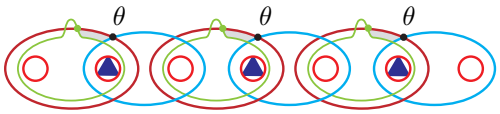

(c) $(D_i, \mathbf{x}_i)$, $i \geq 3$

Figure 6.14: Holomorphic triangles for the β handle-slides

Focusing on the intersection points $\mathbf{x}$ corresponding to the contact element, we see that only the small triangles shown have corners at θ and at $\mathbf{x}$. Therefore, its image under the induced map on homology is simple to compute.

Again restricting our attention to $(D_1, \mathbf{x}_1)$ and $(D_2, \mathbf{x}_2)$, the Heegaard triple for subsequent handle-slides in this sequence is shown in Figure 6.14(b). For $(D_i, \mathbf{x}_i)$, $i \geq 2$, this Heegaard triple diagram is similar to Figure 6.16(c). As before, only small triangles are possible if we are focusing on how the contact element maps under these handle-slides.

The resulting Heegaard diagram and contact invariant after sliding β_0 all the way to the left is as depicted in Figure 6.15. We see that one passes from the original sutured Heegaard diagram to the new one by exchanging β curves, and fixing intersection points which correspond to the contact element.

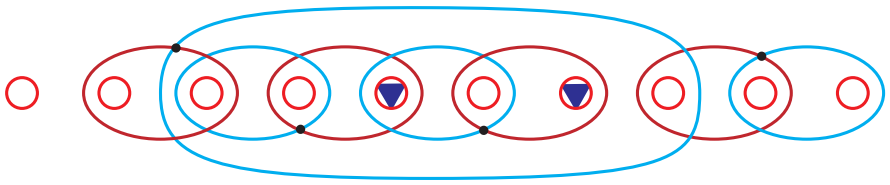

Figure 6.15: Resulting Heegaard diagram after the β handle-slides

We now begin the process of handle-sliding the α_0 curve rightward over what was formerly $(D_2, \mathbf{x}_2)$. For the first such handle-slide, Figures 6.16(a) and 6.16(b) (together with Figure 6.16(c) for $(D_i, \mathbf{x}_i)$, $i > 2$) depict the *two* possible holomorphic triangles with corners at θ and the contact invariant.

Therefore, after this first handle-slide, the contact invariant is mapped to a sum of intersection points. A sensible way of describing this map would be to say that this map sends "(up,down,down,up)" (alternatively, (u, d, d, u)) to the sum $(u, d, d, u) + (d, u, d, u)$. All other intersection points are fixed.

Following through with the second handle-slide, there will now be three holomorphic triangles involved in the map. The first two will be similar to those in Figure 6.16, and will correspond to the mapping $(d, u, d, u) \mapsto (d, u, d, u) + (d, d, u, u)$. The third, shown in Figure 6.17, maps (u, d, d, u) to (u, d, d, u), with all other intersection points fixed.

The final result of this procedure is shown in Figure 6.18. In the end, we see that the intersection

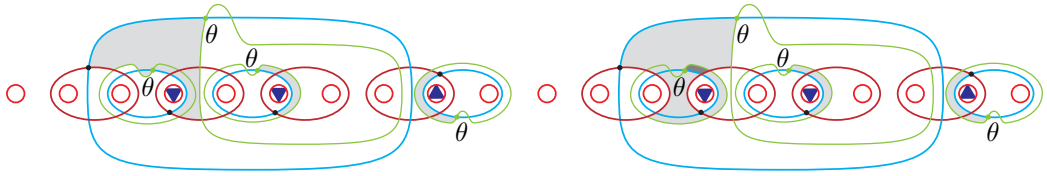

(a) $(D_1, \mathbf{x}_1)$ and $(D_2, \mathbf{x}_2)$, first handle-slide, first holomorphic triangle

(b) $(D_1, \mathbf{x}_1)$ and $(D_2, \mathbf{x}_2)$, first handle-slide, second holomorphic triangle

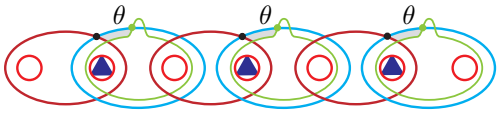

(c) $(D_i, \mathbf{x}_i)$, $i \geq 3$

Figure 6.16: Holomorphic triangles for the first α handle-slide

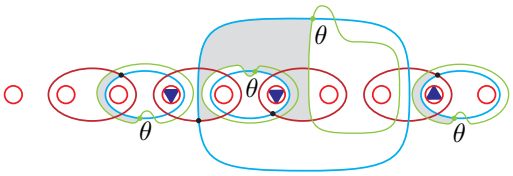

Figure 6.17: An additional holomorphic triangles for subsequent α handle-slides

points (u,d,d,u) are sent to the new collection of intersection points $(u,d,d,u)+(d,u,d,u)+(d,d,u,u)$, which can be obtained from (u,d,d,u) by permuting the first three entries and summing the resulting elements.

Thus, if $(D_2,\mathbf{x}_2)$ has length ℓ, then the resulting sum will have precisely ℓ summands.

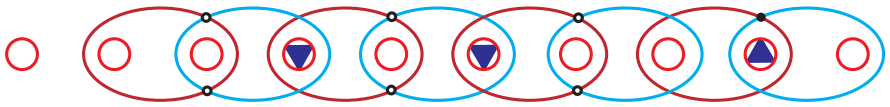

Figure 6.18: Resulting Heegaard diagram after the first sequence of α handle-slides

We repeat this same sequence of handle-slides for $(D_3,\mathbf{x}_3)$ through $(D_k,\mathbf{x}_k)$. It is easy to see that if handle-slides are being performed between "$(D_1,\mathbf{x}_1)$" and $(D_i,\mathbf{x}_i)$, then intersection points corresponding to handle-slides of "$(D_1,\mathbf{x}_1)$" with $(D_j,\mathbf{x}_j)$, $j<i$, are left unchanged. The result is a sum of collection of intersection points.

6.7 Standard Diagrams Part Four

Although the resulting maps on sutured Floer homology in this section are quite different, the sequence of handle-slides performed here are nearly identical to those in Section 6.6.

We can view the handle-slides performed in Section 6.6 as bringing the second stage of our old H2-diagram up to the first or "top" level. In a similar spirit, our goal here is to bring the third stage of our original H2-diagram to this top level. An example is depicted in Figure 6.19.

The process involves handle-sliding the (formerly) stage two β_0 curve repeatedly rightward over the stage three β curves until it become β_0'. Similarly, the α_0 curve is handle-slid repeatedly leftward until it becomes α_0'.

We apply this sequence of handle-slides to each stage three basic H2-diagram, beginning with the leftmost such diagram. As in previous sections, Figures 6.20 and 6.21, together with Figures 6.14(c) and 6.16(c), depict the holomorphic triangles involved in tracking how the contact

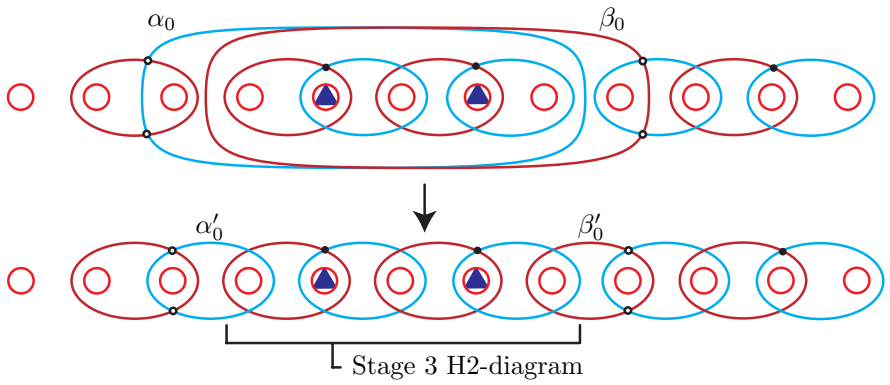

Figure 6.19: Lifting the third stage of an H2-diagram to the top

element maps.

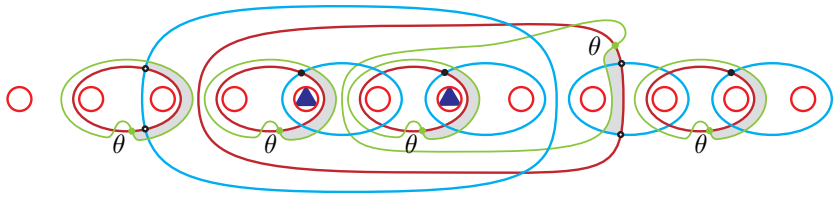

Figure 6.20: Holomorphic triangles for the β handle-slides

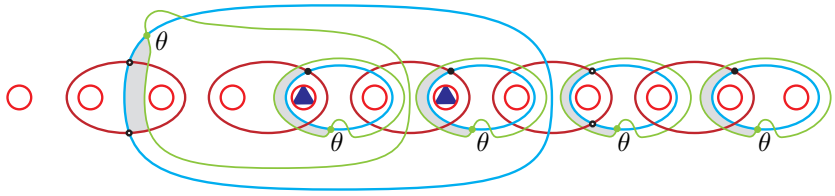

Figure 6.21: Holomorphic triangles for the α handle-slides

Because of the way the α and β curves intersect one another at the stage, the corresponding maps consist only of small triangles. In particular, one passes from the old diagram to the new one by simply exchanging the relevant α and β curves and leaving the intersection points corresponding to the contact element untouched.

The third stage of our original diagram has now been brought, untouched, to the top level. We now apply the handle-slides discussed in the previous two sections to this third-stage. A simple

check shows that vertices coming from stage one and two portions of the original H2-diagram are fixed.

We are now poised to apply the handle-slides discussed in this section and in Section 6.6 to subsequent stages of our original H2-diagram. We observe that as each new odd stage of our original H2-diagram is brought to the top level, intersection points of earlier stages are fixed (only small triangles are allowed for those portions of future Heegaard triples).

6.8 Trees

Here, we complete the proof of Theorem 6 in the special case where the boundary suture (1) is contained in the unbounded region. This is accomplished by describing a straightforward method of tracking the contact element as we pass from an H2-diagram to one in standard form.

To show that each of the resulting contact elements are distinct, we prove that an H2-diagram can be reconstructed from its corresponding contact invariant. This finishes the proof of Theorem 6 in Case 1.

Recall that a general H2-diagram is generated by iteratively replacing receiving sutures by inverted basic H2-diagrams. The information content in specifying a generic H2-diagram can be alternatively captured by a tree with "colored" vertices as shown in Figure 6.22

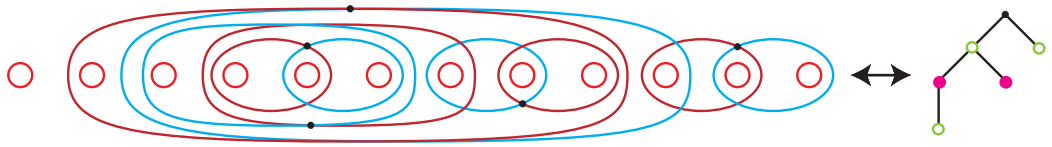

Figure 6.22: Obtaining a colored tree from an H2-diagram

This tree is built iteratively in the same manner as our H1- and H2-diagrams. We have one zeroth level vertex, and one circular first level vertex for each of the receiving regions in the first stage basic H2-diagram. The circular shape is used to indicate that only "up" intersections are possible at this level.

If the i^{th} receiving region of the first stage basic H2-diagram is replaced by a length ℓ basic H2-diagram, then we place ℓ solid vertices below the i^{th} first level vertex and connect these new vertices to their circular parent by edges. Solid vertices are used to indicate that only "down" intersections are possible at even stages.

Iterating this process by using circular vertices for odd stage basic H2-diagrams and solid vertices for even level basic H2-diagrams, we see that an H2-diagram uniquely determines a colored tree and vice versa.

That this tree descends, reflects the fact that the intersection points corresponding to the contact element in an H2-diagram are not initially naturally ordered. We will see a natural ordering emerge as we apply the handle-slides described in Sections 6.6 through 6.7.

Figure 6.23 depicts the handle-slide algorithm defined in Sections 6.6 through 6.7 applied to a specific example. The left-hand side tracks the effect of these handle-slides on the level of sutured Heegaard diagrams, while the right-hand side tracks the resulting changes to the tree.

At various times in the algorithm, natural orderings of vertices appear. We take advantage of this fact by "lifting" relevant vertices up so that they are on the same level and appropriately ordered. As long as edges are kept intact, no information is lost.

The end result is a sum of colored trees, all of whose vertices have been lifted to the same level. Forgetting edges, and only remembering the sequence of circles and dots (corresponding to a sequence of up and down intersections), the result specifies an element in the sutured Floer homology groups of the ambient sutured manifold. The sum of these elements is the contact invariant for that particular H2-diagram.

Final Observation: The process described above can be inverted. In other words, even after throwing away edge information about how vertices are connected, the original graph can be reconstructed from the contact element alone.

Therefore, all the relevant contact elements MUST be unique since their corresponding H2-diagrams are unique.

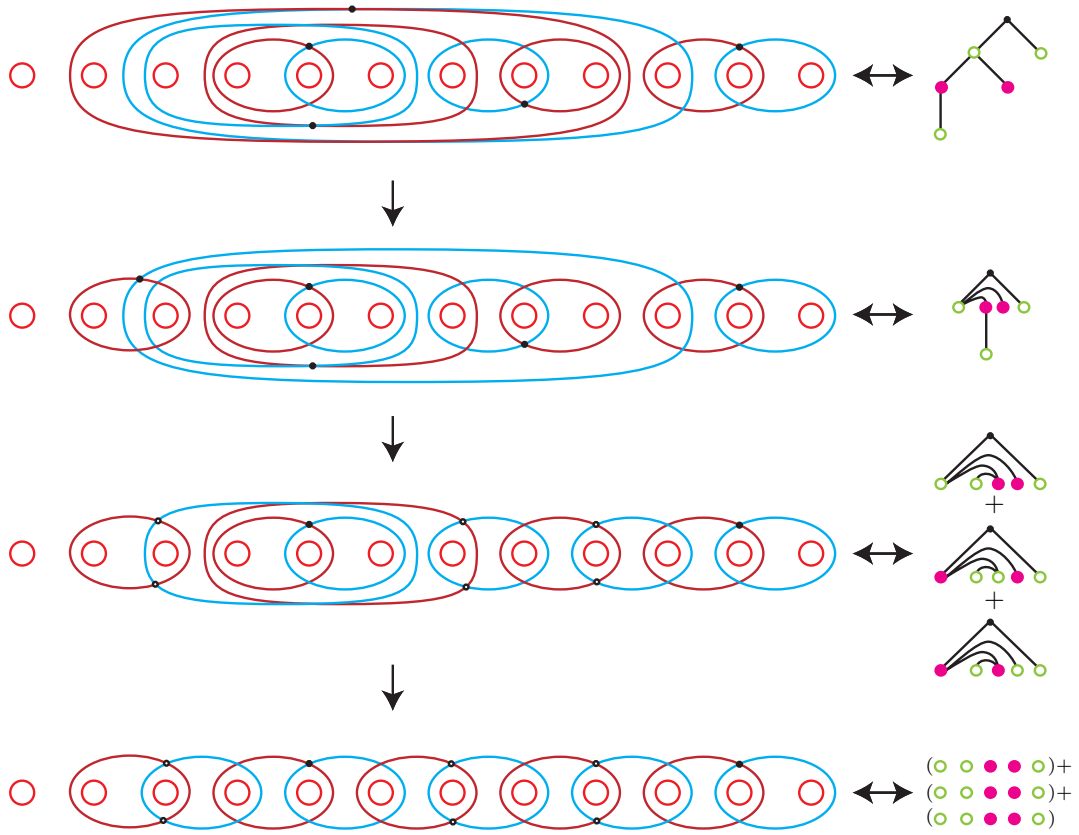

Figure 6.23: Simplifying an H2-diagram and the resulting changes to the tree

Proof of Final Key Observation. Let G be a colored graph coming from some H2-diagram. Consider the collection $\{G_i\}$ of all colored graphs that can be constructed from G by permutations of circular vertices with their solid children.

We can describe an abstract "lifting process" as follows. Fix the position of the zeroth level vertex. Now, from top down, iteratively lift odd-level vertices so that they lie immediately to the right of their parent; lift even-level vertices so that they lie immediately to the left of their parent.

We can apply this abstract lifting process to the collection of graphs contained in $\{G_i\}$ and sum everything together. Forgetting about edges, the result is easily seen to be equal to the contact element obtained above.

Let S be a sum of sequences of circles and dots obtained by applying the above process to some colored graph G. The following steps reverse this process:

Step 1: If every i^{th} element in each summand is circular, draw one small circle on your page along the x-axis (at "hight" $y = 0$), and remove the i^{th} element from each summand.

Remove repeat summands, and repeat this for every "fixed" circle (these correspond to the lowest level circles at the ends of G), each time placing a new circle along the x-axis (matching their order of appearance in each of the summands).

Go to Step 5 if the sum is empty.

Step 2: Look for a summand with two circles side-by-side, say the i^{th} and $(i+1)^{\text{st}}$ elements in this summand. Now progress rightward through each summand finding the next instance where two circles occur side-by-side, say the k^{th} and $(k+1)$st elements. Now place $i-k-1$ solid dots at height $y = 1$ and one small circle above them at height $y = 2$. Add edges from this circle down to each of the solid dots. Now remove the $(i+1)$st through k^{th} dots from each summand.

If any of the circles removed in Step 1 fell between the removed dots, place an edge connecting that green dot to its "former" right neighbor.

Remove any repeat summands. Go to Step 5 if no dots remain.

Step 3: Repeat the procedure described in Step 2, now placing the new solid dots one level

above the previously placed circles, and the new circles one level above the new solid dots.

If any of the previously removed collections of circles and dots fell between newly removed circles and dots, place an edge connecting the top circle to their "former" right neighbor.

Step 4: If elements remain in the sum, go back to Step 3; otherwise, go to Step 5.

Step 5: Place one black dot above all others and connect it by edges to any circles with no solid dots above them

The resulting colored tree is G.

□

6.9 Three Main Cases

We are now poised to finish the proof of our main theorem. The problem can be broken into three main cases.

Case 1: *In the H2-diagram, the number 1 suture is contained in the unbounded region.*

This is precisely the case that was handled in Sections 6.5 through 6.8, where we saw that each of the resulting contact invariants must be pairwise distinct.

Case 2: *In the H2-diagram, the number 2 suture is contained in the unbounded region.*

Rotate the H2-diagram by 180 degrees. The result will be a diagram similar to that in Case 1, but with the orders of sutures reversed. By an analysis similar to that in Case 1, we conclude that each of the contact invariants in this Case are pairwise distinct. What remains is to check that each of these elements are distinct from those in Case 1. To see that this is the case, consider Figure 6.24.

In the top portion of Figure 6.24, we see an example of an H2-diagram from Case 2. Next, in the middle of that same figure, we see the same diagram after an isotopy which sends the β_0 curve around the other side of the spherical Heegaard surface. Last, the bottom portion of this Figure 6.24 depicts that same sutured Heegaard diagram after handle-sliding the β_0 curve leftward

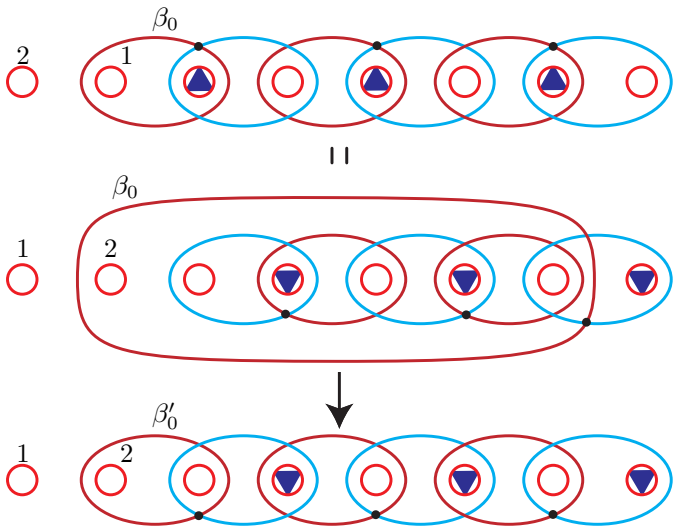

Figure 6.24: First simplification to an H2-diagram from Case 2

until it becomes β_0' and swallows only the second and third boundary sutures.

A simple computation, like that in Section 6.2, shows that this sequence of handle-slides maps the contact invariant as shown in the bottom of Figure 6.25, leaving intersections at subsequent stages of this diagram untouched.

The key observation is that if we now put this diagram into standard form, the contact element will be a sum of collections of intersection points, each beginning with a "down" intersection. This cannot happen in Case 1.

Case 3: *In the H2-diagram, neither the number 1, nor the number 2 sutures are contained in the unbounded region.*

By an argument similar to that in Cases 1 and 2, it follows that distinct H2-diagrams falling into Case 3 produce distinct contact invariants. As in Case 2, what remains to be seen is that each these contact invariants are, in turn, also distinct from those in Cases 1 and 2. To see this is the case, consider Figure 6.25.

In the top portion of Figure 6.25, we see an example of an H2-diagram falling into Case 3. Next, in the middle of that same figure, we see that diagram after an isotopy sending the β_0

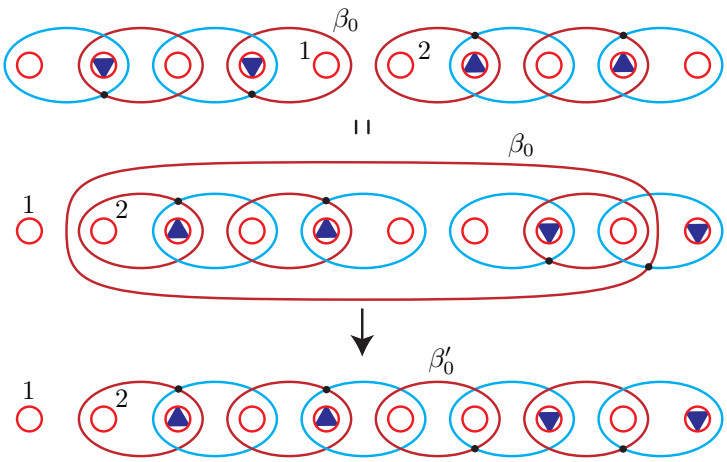

Figure 6.25: First simplification to an H2-diagram from Case 3

curve around the other side of the spherical Heegaard surface. Last, the bottom portion of this Figure 6.24 depicts that same sutured Heegaard diagram after handle-sliding the β_0 curve leftward and rightward until it becomes β_0' and swallows only two boundary sutures in the middle.

A computation like those in previous sections shows that this sequence of handle-slides maps the contact invariant as shown in the bottom of Figure 6.25. Again, the maps induced by this sequence of handle-slides leave the intersections corresponding to the contact element at subsequent stages of this diagram untouched.

What distinguishes the contact elements in this case from those in Case 1 is that if we now put this diagram into standard form, the contact element will be a sum of intersection points, all having at least one common "down" intersection. This cannot happen in Case 1. However, although each collection of intersection points in this sum has a common "down" intersection, it cannot be the first intersection. Thus, contact elements coming from diagrams in Case 3 cannot agree with those coming from Case 2.

This concludes the proof of Theorem 6.

□

Bibliography

[Col99] Vincent Colin, *Recollement de variétés de contact tendues*, Bull. Soc. Math. France **127** (1999), no. 1, 43–69.

[Col07] ———, *Ouverts en géométrie de contact [d'aprés emmanuel giroux]*, Séminaire Bourbaki, 59 ème année (2006-2007), no. 969, to appear in Asterisque.

[EFM01] Judith Epstein, Dmitry Fuchs, and Maike Meyer, *Chekanov-Eliashberg invariants and transverse approximations of Legendrian knots*, Pacific J. Math. **201** (2001), no. 1, 89–106.

[EH01] John B. Etnyre and Ko Honda, *Knots and contact geometry. I. Torus knots and the figure eight knot*, J. Symplectic Geom. **1** (2001), no. 1, 63–120.

[Etn05] John B. Etnyre, *Legendrian and transversal knots*, Handbook of knot theory, Elsevier B. V., Amsterdam, 2005, pp. 105–185.

[Etn06] ———, *Lectures on open book decompositions and contact structures*, Floer Homology, Gauge Theory, and Low-dimensional Topology, Clay Math. Proc., vol. 5, Amer. Math. Soc., Providence, RI, 2006, pp. 103–141.

[EV08] John B. Etnyre and David Shea Vela-Vick, *Legendrian and transverse link invariants*, Preprint, 2008.

[GHV07] Paolo Ghiggini, Ko Honda, and Jeremy Van Horn-Morris, *The vanishing of the contact invariant in the presence of torsion*, Preprint, arXiv:0706.1602v2 [math.GT], 2007.

[Gir00] Emmanuel Giroux, *Structures de contact en dimension trois et bifurcations des feuilletages de surfaces*, Invent. Math. **141** (2000), no. 3, 615–689.

[Gir02] ———, *Géométrie de contact: de la dimension trois vers les dimensions supérieures*, Proceedings of the International Congress of Mathematicians, Vol. II (Beijing, 2002) (Beijing), Higher Ed. Press, 2002, pp. 405–414.

[HKM06] Ko Honda, William Kazez, and Gordana Matič, *On the contact class in Heegaard Floer homology*, Preprint, arXiv:math/0609734v2 [math.GT], 2006.

[HKM07] ———, *On the contact invariant in sutured Floer homology*, Preprint, arXiv:math/0705.2828v2 [math.GT], 2007.

[HKM08] ———, *Contact structures, sutured Floer homology, and TQFT*, Preprint, arXiv:math/0807.2431v1[math.GT], 2008.

[Hon00] Ko Honda, *On the classification of tight contact structures. I*, Geom. Topol. **4** (2000), 309–368 (electronic).

[Juh06] András Juhász, *Holomorphic discs and sutured manifolds*, Algebr. Geom. Topol. **6** (2006), 1429–1457 (electronic).

[Juh08] ———, *Floer homology and surface decompositions*, Geom. Topol. **12** (2008), no. 1, 299–350.

[Lip06] Robert Lipshitz, *A cylindrical reformulation of Heegaard Floer homology*, Geom. Topol. **10** (2006), 955–1097 (electronic).

[LOSS08] Paolo Lisca, Peter Ozsváth, András I. Stipsicz, and Zoltán Szabó, *Heegaard Floer invariants of Legendrian knots in contact three-manifolds*, Preprint, `arXiv:0802.0628v1` [math.SG], 2008.

[OS04a] Peter Ozsváth and Zoltán Szabó, *Holomorphic disks and knot invariants*, Adv. Math. **186** (2004), no. 1, 58–116.

[OS04b] ———, *Holomorphic disks and three-manifold invariants: properties and applications*, Ann. of Math. (2) **159** (2004), no. 3, 1159–1245.

[OS04c] ———, *Holomorphic disks and topological invariants for closed three-manifolds*, Ann. of Math. (2) **159** (2004), no. 3, 1027–1158.

[OS05a] ———, *Heegaard Floer homology and contact structures*, Duke Math. J. **129** (2005), no. 1, 39–61.

[OS05b] ———, *Holomorphic disks, link invariants, and the multi-variable alexander polynomial*, Preprint, `arXiv:math/0512286v2`[math.GT], 2005.

[OS08a] Peter Ozsváth and András I. Stipsicz, *Contact surgeries and the transverse invariant in knot Floer homology*, Preprint, `arXiv:0803.1252v1` [math.SG], 2008.

[OS08b] Peter Ozsváth and Zoltán Szabó, *Link Floer homology and the Thurston norm*, J. Amer. Math. Soc. **21** (2008), no. 3, 671–709.

[Ras03] Jacob Rasmussen, *Floer homology and knot complements*, Ph.D. thesis, Harvard University, 2003, `arXiv:math/0306378v1` [math.GT].

[SV08] András I. Stipsicz and Vera Vértesi, *On invariants for Legendrian knots*, Preprint, `arXiv:0806.1436v1`[math.GT], 2008.

[Tor00] Ichiro Torisu, *Convex contact structures and fibered links in 3-manifolds*, Internat. Math. Res. Notices (2000), no. 9, 441–454.

[TW75] William P. Thurston and Horst E. Winkelnkemper, *On the existence of contact forms*, Proc. Amer. Math. Soc. **52** (1975), 345–347.

[Vel08] David Shea Vela-Vick, *On the transverse invariant for bindings of open books*, Preprint, `arXiv:0806.1729v1`[math.SG], 2008.